ESAIM: M2AN 59 (2025) 2739–2761
https://doi.org/10.1051/m2an/2025071

ESAIM: Mathematical Modelling and Numerical Analysis
www.esaim-m2an.org

UNCONDITIONALLY STABLE, LINEARISED IMEX SCHEMES FOR INCOMPRESSIBLE FLOWS WITH VARIABLE DENSITY

Nicolás Espinoza-Contreras[1,2,3], Gabriel R. Barrenechea[4], Ernesto Castillo[5] and Douglas R. Q. Pacheco[1,2,3,*]

Abstract. For the incompressible Navier–Stokes system with variable viscosity and density, we propose and analyse an IMEX framework treating the convective and diffusive terms semi-implicitly. This extends to variable density and second order in time some methods previously analysed for variable viscosity and constant density. We present three new schemes, one of which is a fully decoupled fractional-step method. All of them share the novelty that the viscous term is treated in an implicit-explicit (IMEX) fashion which, if combined with an explicit treatment of the pressure, decouples the velocity components. Unconditional temporal stability is proved for all three variants. Furthermore, the system to solve at each time step is linear, thus avoiding the costly solution of nonlinear problems even if the viscosity follows a non-Newtonian rheological law. Our presentation is restricted to the semi-discrete case, only considering the time discretisation. In this way, the results herein can be applied to any spatial discretisation. We validate our theory through numerical experiments considering finite element methods in space. The tests range from simple manufactured solutions to complex two-phase viscoplastic flows.

Mathematics Subject Classification. 65M12, 65M22, 65M60, 76D05, 76T99.

Received October 27, 2024. Accepted August 12, 2025.

1. Introduction

In incompressible flows, density variability occurs mainly in the presence of different fluid phases, be they immiscible or not. Since the seminal work by Guermond and Quartapelle [1], many numerical methods have been developed for the incompressible variable-density Navier–Stokes equations. Most works devoted to the numerical analysis of problems with variable density (*e.g.*, [1–5]) assume constant viscosity, which facilitates the analysis and makes it simpler to discretise the viscous term implicitly. However, since the dynamic viscosity is proportional to the density and since different fluids have different kinematic viscosities, variable density will,

Keywords and phrases. Multiphase flow, interface capturing, variable density, generalised Newtonian fluids, incremental pressure correction, projection methods.

[1] Chair for Computational Analysis of Technical Systems, RWTH Aachen University, Aachen, Germany.

[2] Chair of Methods for Model-based Development in Computational Engineering, RWTH Aachen University, Aachen, Germany.

[3] Center for Simulation and Data Science (JARA-CSD), RWTH Aachen University, Aachen, Germany.

[4] Department of Mathematics and Statistics, University of Strathclyde, Glasgow, Scotland.

[5] Department of Mechanical Engineering, University of Santiago de Chile, Santiago, Chile.

*Corresponding author: pacheco@ssd.rwth-aachen.de

© The authors. Published by EDP Sciences, SMAI 2025

This is an Open Access article distributed under the terms of the Creative Commons Attribution License (https://creativecommons.org/licenses/by/4.0), which permits unrestricted use, distribution, and reproduction in any medium, provided the original work is properly cited.

in practice, also imply variable viscosity. Therefore, this work shall also address non-constant viscosity and how to handle it numerically to preserve the desirable algorithmic properties attained for homogeneous flows.

For problems with variable density, decoupling strategies are usually preferred over monolithic discretisations: density-momentum decoupling is the standard in variable-density solvers, with pressure segregation also being a very common approach. There is a vast body of literature on corresponding fractional-step schemes, and we can sort most of these methods into three families. The first are incremental pressure-correction schemes [1,6], which are variable-density extensions of classical projection methods; the second family are Gauge–Uzawa schemes [4, 7, 8], which also belong to the class of projection methods; the third popular approach is penalty methods, which perturb the incompressibility constraint using an incremental pressure Laplacian [2,9–13]. The advantages of the latter are their constant-coefficient pressure equation and their stable second-order version [2]; for the other two families (projection methods), no second-order extensions have yet been proven stable, although numerical evidence often indicates good stability [1,7,14]. A less common, yet very accurate alternative, is consistent splitting schemes, which are based on a fully consistent pressure equation and therefore eliminate splitting errors and numerical boundary layers [15,16]. Finally, an important issue is that, in the variable-density context, pressure-correction methods usually require solving two pressure Poisson problems per time step [1]. A variant requiring only one pressure solve per time step was recently proposed [6] and is the approach we also follow.

In this work, our main goal is to propose and analyse IMEX schemes. In CFD, the term IMEX usually refers to temporal discretisations that make convection (semi-)explicit and keep viscous terms implicit [17–21]. For variable density, too, most of the literature treats the convective term semi-implicitly to linearise the momentum equation and decouple the density update from the velocity-pressure step [1]. Now, when density is not constant, neither is viscosity, so the diffusive term cannot be written as a simple vector Laplacian. Consequently, implicit treatments will end up coupling all the velocity components, even if a pressure segregation method is used. These considerations motivate the search for techniques that decouple the velocity components and lead to schemes in which only one linear system per unknown is required at each time step. Thus, IMEX discretisations that make the transpose velocity gradient or other coupling terms explicit have both theoretical and practical relevance. This was the main motivation for our recent work [22], where first-order IMEX schemes built under this premise were analysed for problems with variable viscosity (but constant density). To the best of our knowledge, not many works to date are devoted to IMEX schemes for non-homogeneous flows [23–25]. The present work generalises our recent approach to the variable-density case and also presents a second-order extension. We propose three different IMEX methods: a first- and a second-order method decoupling only density transport and momentum, and a first-order projection method fully decoupling density, pressure, and velocity (components). We shall prove that all of our schemes, which are based on a consistent reformulation of the viscous term, are unconditionally stable in time.

The rest of this manuscript is organised as follows. Section 2 introduces the model problem and underlying assumptions, as well as useful notation, identities and inequalities. Section 3 presents our new IMEX schemes, whose temporal stability is then analysed in Section 4. Section 5 briefly addresses implementation matters, followed by numerical examples in Section 6. We finally draw concluding remarks in Section 7.

2. Preliminaries

2.1. Model problem

For a finite time interval $(0, T]$ and a domain $\Omega \subset \mathbb{R}^d$, $d = 2$ or 3, the variable-density incompressible Navier–Stokes equations can be written as

$$\partial_t \rho + \boldsymbol{u} \cdot \nabla \rho = 0 \qquad \text{in } \Omega \times (0, T] =: Q, \tag{1}$$

$$\rho \partial_t \boldsymbol{u} + (\rho \nabla \boldsymbol{u})\boldsymbol{u} - \nabla \cdot (2\mu \nabla^{\mathrm{s}} \boldsymbol{u}) + \nabla p = \boldsymbol{f} \qquad \text{in } \Omega \times (0, T], \tag{2}$$

$$\nabla \cdot \boldsymbol{u} = 0 \qquad \text{in } \Omega \times (0, T], \tag{3}$$

where $\boldsymbol{u}$ is the velocity, p is the pressure, ρ is the density, $\boldsymbol{f}$ is a body force, and μ is the dynamic viscosity, which is assumed to satisfy

$$0 < \mu_{\min} \leq \mu \leq \mu_{\max} \text{ in } \bar{Q}, \tag{4}$$

where $\mu_{\min}$ and $\mu_{\max}$ are constants usually determined by fluid properties (density and rheology). Initial and boundary conditions are also needed, which depend on the application, see *e.g.*, reference [16]. For the theoretical analysis, we will consider $\boldsymbol{u} = \boldsymbol{0}$ on $\partial\Omega$, so no boundary conditions are needed for ρ. In this case, if the initial density field $\rho_0(\boldsymbol{x})$ is such that $0 < \rho_{\min} \leq \rho_0(\boldsymbol{x}) \leq \rho_{\max}$ for all $\boldsymbol{x} \in \Omega$, then [1]

$$\rho_{\min} \leq \rho(\boldsymbol{x}, t) \leq \rho_{\max} \text{ in } \bar{Q}. \tag{5}$$

2.2. Consistent reformulation

When μ can vary in space, the viscous term cannot be simplified to the Laplacian form $\mu\Delta\boldsymbol{u}$. On the other hand, the natural writing of the diffusive term, namely the stress-divergence form

$$\nabla \cdot (2\mu\nabla^{\mathrm{s}}\boldsymbol{u}) = \nabla \cdot (\mu\nabla\boldsymbol{u}) + \nabla \cdot \left(\mu\nabla^{\top}\boldsymbol{u}\right), \tag{6}$$

has computational disadvantages. In fact, the second term (the transpose gradient) couples the different components u^j of the velocity, since the ith entry in the vector $\nabla \cdot (\mu\nabla^{\top}\boldsymbol{u})$ involves all u^j components, $j = 1, \ldots, d$. This does not happen for the first term in (6) because the ith entry in $\nabla \cdot (\mu\nabla\boldsymbol{u})$ is simply $\nabla \cdot (\mu\nabla u^i)$ – which is the reason why the Laplacian form is often preferred for dicretisation (when μ is constant). In principle, the coupling could be avoided by treating the transpose gradient explicitly, but we have recently shown that this is generally unstable [22]. To overcome that, we use the following consistent reformulation:

$$\begin{aligned} \nabla \cdot (2\mu\nabla^{\mathrm{s}}\boldsymbol{u}) &\equiv \nabla \cdot (\mu\nabla\boldsymbol{u}) + \nabla^{\top}\boldsymbol{u}\nabla\mu + \mu\nabla(\nabla \cdot \boldsymbol{u}) \\ &= \nabla \cdot (\mu\nabla\boldsymbol{u}) + \nabla^{\top}\boldsymbol{u}\nabla\mu, \end{aligned} \tag{7}$$

which we call *generalised Laplacian* form. The term $\nabla \cdot (\mu\nabla\boldsymbol{u})$ is a variable-coefficient Laplacian, which at the fully discrete level leads to block-diagonal velocity matrices. In this context, our idea is to treat explicitly $\nabla^{\top}\boldsymbol{u}$ and possibly μ (if the viscosity follows some non-Newtonian law), analysing also the implications of such an IMEX approach. In the analysis presented below, we will assume that

$$\nabla\mu \in \left[L^{\infty}(\bar{Q})\right]^d, \tag{8}$$

which is essentially a Lipschitz condition on μ.

For numerical stability, Guermond and Quartapelle [1] proposed an equivalent rewriting of the strong equations. Combining that rewriting with (7) leads to the following formulation:

$$\partial_t\rho + \boldsymbol{u} \cdot \nabla\rho + \frac{\nabla \cdot \boldsymbol{u}}{2}\rho = 0, \tag{9}$$

$$\sqrt{\rho}\,\partial_t\left(\sqrt{\rho}\boldsymbol{u}\right) + (\rho\nabla\boldsymbol{u})\,\boldsymbol{u} + \frac{1}{2}\left[\nabla \cdot (\rho\boldsymbol{u})\right]\boldsymbol{u} - \nabla \cdot (\mu\nabla\boldsymbol{u}) - \nabla^{\top}\boldsymbol{u}\nabla\mu + \nabla p = \boldsymbol{f}, \tag{10}$$

$$\nabla \cdot \boldsymbol{u} = 0, \tag{11}$$

which is equivalent to (1)–(3).

2.3. Useful notation, identities and inequalities

We consider usual notation for Sobolev, Hilbert and Lebesgue spaces [26]. The inner product in $L^2(\Omega)$ and duality pairing in $H^{-1}(\Omega) \times H_0^1(\Omega)$ are denoted by $(\cdot, \cdot)$ and $\langle\cdot, \cdot\rangle$, respectively; no distinction is made between the product of scalar, vector- or tensor-valued functions. Moreover, we denote by $\|\cdot\|$, $\|\cdot\|_{-1}$ and $\|\cdot\|_{\infty}$ the

$L^2(\Omega)$, $H^{-1}(\Omega)$ and $L^\infty(\bar{Q})$ norms, respectively. We assume that $\boldsymbol{f} \in [H^{-1}(\Omega)]^d$ for all t and that the initial velocity data satisfies $\boldsymbol{u}_0 \in [H_0^1(\Omega)]^d$. To shorten notation, we define $\boldsymbol{U} := \sqrt{\rho}\,\boldsymbol{u}$.

In our analysis, approximate or discrete-in-time values of the quantities at the different time steps will be denoted with sub-indices: $\boldsymbol{u}_n$, for instance, denotes the velocity approximation at the nth time step. The following identities will be useful:

$$2(\boldsymbol{v}_{n+1} - \boldsymbol{v}_n, \boldsymbol{v}_{n+1}) = \|\boldsymbol{v}_{n+1}\|^2 - \|\boldsymbol{v}_n\|^2 + \|\delta\boldsymbol{v}_{n+1}\|^2, \tag{12}$$

$$2(3\boldsymbol{v}_{n+1} - 4\boldsymbol{v}_n + \boldsymbol{v}_{n-1}, \boldsymbol{v}_{n+1}) = \|\boldsymbol{v}_{n+1}\|^2 - \|\boldsymbol{v}_n\|^2 + \|\boldsymbol{v}_{n+1}^\star\|^2 - \|\boldsymbol{v}_n^\star\|^2 + \|\delta^2\boldsymbol{v}_{n+1}\|^2, \tag{13}$$

which hold for any scalar or vector-valued $\boldsymbol{v}_{n+1}, \boldsymbol{v}_n, \boldsymbol{v}_{n-1}$, where

$$\begin{aligned}
\boldsymbol{v}_{n+1}^\star &:= 2\boldsymbol{v}_{n+1} - \boldsymbol{v}_n,\\
\delta\boldsymbol{v}_{n+1} &:= \boldsymbol{v}_{n+1} - \boldsymbol{v}_n,\\
\delta^2\boldsymbol{v}_{n+1} &:= \boldsymbol{v}_{n+1} - 2\boldsymbol{v}_n + \boldsymbol{v}_{n-1} = \boldsymbol{v}_{n+1} - \boldsymbol{v}_n^\star.
\end{aligned}$$

Another important fact is the skew-symmetry of the convective terms. For any $(r, \boldsymbol{v}, \boldsymbol{w})$ sufficiently smooth, there hold

$$\int_\Omega \left[\boldsymbol{v}\cdot\nabla r + \frac{\nabla\cdot\boldsymbol{v}}{2} r\right] r\,\mathrm{d}\Omega = 0, \tag{14}$$

$$\int_\Omega \left[(r\nabla\boldsymbol{v})\boldsymbol{w} + \frac{\nabla\cdot(r\boldsymbol{w})}{2}\boldsymbol{v}\right]\cdot\boldsymbol{v}\,\mathrm{d}\Omega = 0, \tag{15}$$

provided that $\boldsymbol{v}\cdot\boldsymbol{n} = 0$ on $\partial\Omega$ [1].

We will analyse both coupled and fractional-step schemes. The stability analysis will rely on the following Gronwall inequality, proved by Heywood and Rannacher [27].

Lemma 2.1 (Discrete Gronwall inequality)**.** *Let $N \in \mathbb{N}$, and α, B, a_n, b_n, c_n be non-negative numbers for $n = 1, \ldots, N$. Let us suppose that these numbers satisfy*

$$a_N + \sum_{n=1}^N b_n \le B + \sum_{n=1}^N c_n + \alpha\sum_{n=1}^{N-1} a_n. \tag{16}$$

Then, the following inequality holds:

$$a_N + \sum_{n=1}^N b_n \le \mathrm{e}^{\alpha N}\left(B + \sum_{n=1}^N c_n\right) \quad \text{for} \quad N \ge 1. \tag{17}$$

IMEX stepping schemes can be constructed by using backward differentiation formulas (BDFs) and extrapolation rules of matching order. We will consider first- and second-order schemes, for which we have

$$\begin{aligned}
\text{1st order:}\quad \partial_t\left(\sqrt{\rho}\,\boldsymbol{u}\right)|_{t=t_{n+1}} &\approx \frac{1}{\tau}\left(\sqrt{\rho_{n+1}}\,\boldsymbol{u}_{n+1} - \sqrt{\rho_n}\,\boldsymbol{u}_n\right)\\
\boldsymbol{u}_{n+1} &\approx \boldsymbol{u}_n\\
\text{2nd order:}\quad \partial_t\left(\sqrt{\rho}\,\boldsymbol{u}\right)|_{t=t_{n+1}} &\approx \frac{1}{2\tau}\left(3\sqrt{\rho_{n+1}}\,\boldsymbol{u}_{n+1} - 4\sqrt{\rho_n}\,\boldsymbol{u}_n + \sqrt{\rho_{n-1}}\,\boldsymbol{u}_{n-1}\right)\\
\boldsymbol{u}_{n+1} &\approx 2\boldsymbol{u}_n - \boldsymbol{u}_{n-1} = \boldsymbol{u}_n^\star,
\end{aligned}$$

where $\tau = T/N > 0$ denotes a constant time-step size, for simplicity. Similarly, the density equation (9) will be solved for ρ_{n+1} either *via*

$$\frac{\rho_{n+1} - \rho_n}{\tau} + \boldsymbol{u}_n\cdot\nabla\rho_{n+1} + \frac{\nabla\cdot\boldsymbol{u}_n}{2}\rho_{n+1} = 0, \tag{18}$$

or through the second-order scheme

$$\frac{3\rho_{n+1} - 4\rho_n + \rho_{n-1}}{2\tau} + \boldsymbol{u}_n^\star \cdot \nabla \rho_{n+1} + \frac{\nabla \cdot \boldsymbol{u}_n^\star}{2} \rho_{n+1} = 0. \tag{19}$$

We will assume that the numerical density ρ_n is bounded as

$$\varrho_{\min} \leq \rho_n \leq \varrho_{\max} < \infty \text{ a.e. in } \Omega, \qquad \forall n = 0, \ldots, N, \tag{20}$$

where $\varrho_{\min}$ is a constant in $(0, \rho_{\min}]$.

Remark 2.1. As stated by Guermond and Salgado [2, 9], assumption (20) can be proven in the context of the semi-discrete analysis we carry out in this work. We start by defining the positive and negative parts of a function $v \in H^1(\Omega)$, a.e. in Ω, by

$$v^+(\boldsymbol{x}) = \max\{v(\boldsymbol{x}), 0\} \quad \text{and} \quad v^-(\boldsymbol{x}) = v(\boldsymbol{x}) - v^+(\boldsymbol{x}).$$

Then, if we assume that $\rho_n \geq \rho_{\min}$, multiplying (18) by $\tau(\rho_{n+1} - \rho_{\min})^-$, integrating over Ω, using the fact that $\boldsymbol{u}_n$ is solenoidal and vanishes on the boundary (thus the convective term is skew-symmetric) and that v^+ and v^- have complementary supports in Ω, we arrive at the following:

$$\begin{aligned}\int_\Omega \left[(\rho_{n+1} - \rho_{\min})^-\right]^2 \, \mathrm{d}\Omega = \int_\Omega (\rho_n - \rho_{\min}) (\rho_{n+1} - \rho_{\min})^- \, \mathrm{d}\Omega \\ \leq 0,\end{aligned}$$

and then (20) follows with $\varrho_{\min} = \rho_{\min}$. Up to our best knowledge, the same proof cannot be repeated for the second-order scheme based on (19). In addition, in the fully discrete case, the proof sketched above may no longer hold. In both these situations, possible ways of deriving a discretisation that guarantees (20) include either methods related to the FCT scheme [28] or the ones reviewed in recent monographs [29,30]. Alternatively, we could use a penalisation such as the one proposed by Burman and Ern [31] to impose (20) weakly. One final option is to use a more recent method [32] where the restriction (20) would be hardwired into the method regardless of the space or time discretisation.

3. Iteration-free IMEX methods

In this article, we propose three different IMEX schemes. For the first two methods, velocity and pressure are computed simultaneously at each time step, after the density is updated through either (18) or (19). Whenever the term "coupled scheme" is used herein, we mean the coupling between pressure and velocity; the density, on the other hand, will always be computed separately (beforehand) at each time step. Another common feature of all the methods presented herein is being fully linearised, *i.e.*, each time step requires solving only linear systems.

3.1. A first-order coupled scheme

To derive a first-order linearised scheme, we use BDF1 for the time derivatives and extrapolate selected terms. The density is first updated *via* (18), followed by the velocity-pressure step:

$$\begin{aligned}&\frac{\sqrt{\rho_{n+1}}}{\tau} \left(\sqrt{\rho_{n+1}}\, \boldsymbol{u}_{n+1} - \sqrt{\rho_n}\, \boldsymbol{u}_n\right) + \left(\rho_{n+1} \nabla \boldsymbol{u}_{n+1}\right) \boldsymbol{u}_n + \frac{1}{2} \left[\nabla \cdot (\rho_{n+1} \boldsymbol{u}_n)\right] \boldsymbol{u}_{n+1} \\ &\quad - \nabla \cdot (\mu_{n+1} \nabla \boldsymbol{u}_{n+1}) + \nabla p_{n+1} = \nabla^\top \boldsymbol{u}_n \nabla \mu_{n+1} + \boldsymbol{f}_{n+1}, \qquad (21)\\ &\nabla \cdot \boldsymbol{u}_{n+1} = 0. \qquad (22)\end{aligned}$$

Remark 3.1. This scheme assumes that μ_{n+1} is already known at the point of computing $\boldsymbol{u}_{n+1}$ and p_{n+1}. This is often the case since the viscosity field is normally propagated with ρ, that is, $\mu_{n+1} = f(\rho_{n+1})$. In non-Newtonian applications, however, the viscosity may further depend locally on $\nabla^{\mathrm{s}}\boldsymbol{u}$ or p. In that case, we can avoid the nonlinearity by simply replacing μ_{n+1} with μ_n in equation (21), which does not affect the unconditional stability of the scheme. A more detailed discussion of the non-Newtonian case is given in Section 5.

3.2. A second-order coupled scheme

To extend the method to order two in time, we switch to BDF2 and second-order extrapolations. After computing ρ_{n+1} through (19), we update velocity and pressure *via*

$$\begin{aligned}
&\frac{\sqrt{\rho_{n+1}}}{2\tau}\left(3\sqrt{\rho_{n+1}}\,\boldsymbol{u}_{n+1} - 4\sqrt{\rho_n}\,\boldsymbol{u}_n + \sqrt{\rho_{n-1}}\,\boldsymbol{u}_{n-1}\right) + (\rho_{n+1}\nabla\boldsymbol{u}_{n+1})\boldsymbol{u}_n^\star + \frac{1}{2}\left[\nabla\cdot(\rho_{n+1}\boldsymbol{u}_n^\star)\right]\boldsymbol{u}_{n+1} \\
&\qquad - \nabla\cdot(\mu_{n+1}\nabla\boldsymbol{u}_{n+1}) + \nabla p_{n+1} = \nabla^\top\boldsymbol{u}_n^\star\nabla\mu_{n+1} + \boldsymbol{f}_{n+1}, \qquad (23)\\
&\nabla\cdot\boldsymbol{u}_{n+1} = 0. \qquad (24)
\end{aligned}$$

As in the first-order case, μ_{n+1} can be replaced by a suitable extrapolation – now second-order – if the viscosity follows a nonlinear rheology (see Sect. 5).

Remark 3.2. Since this is a multi-step method, we use a single first-order step as initialisation to compute $\rho_1, \boldsymbol{u}_1, p_1$. This is a standard approach, and the numerical evidence available strongly suggests that it does not affect the (global-in-time) second order of the scheme.

3.3. A first-order fractional-step scheme

Our IMEX treatment of the viscous term is especially advantageous when also segregating the pressure because, in that case, the resulting scheme will only require the solution of *scalar* subproblems: one for the pressure and one for each velocity component. For this, we propose an IMEX modification of the incremental pressure-correction method by Deteix *et al.* [6], who originally considered a fully implicit treatment of the convective and viscous terms. While classical projection methods for variable-density flows [1] require solving two pressure Poisson equations per time step, this variant requires only one, which is why it is our framework of choice here. We propose the following method:

- **Step 0:** To initialise the algorithm, set $\hat{\mathbf{u}}_0 = \boldsymbol{u}_0$ and provide (an approximation for) p_0.
- **Step 1:** Find ρ_{n+1} as the solution of

$$\frac{\rho_{n+1}-\rho_n}{\tau} + \hat{\mathbf{u}}_n\cdot\nabla\rho_{n+1} + \frac{\nabla\cdot\hat{\mathbf{u}}_n}{2}\rho_{n+1} = 0. \qquad (25)$$

- **Step 2:** Find the velocity $\boldsymbol{u}_{n+1}$ by solving

$$\begin{cases}
\frac{\rho_{n+1}}{\tau}\boldsymbol{u}_{n+1} + (\rho_{n+1}\nabla\boldsymbol{u}_{n+1})\boldsymbol{u}_n + \frac{1}{2}[\nabla\cdot(\rho_{n+1}\boldsymbol{u}_n)]\boldsymbol{u}_{n+1} - \nabla\cdot(\mu_{n+1}\nabla\boldsymbol{u}_{n+1}) \\
\qquad = \frac{\sqrt{\rho_{n+1}\rho_n}}{\tau}\hat{\mathbf{u}}_n - \sqrt{\frac{\rho_{n+1}}{\rho_n}}\nabla p_n + \nabla^\top\boldsymbol{u}_n\nabla\mu_{n+1} + \boldsymbol{f}_{n+1}, \\
\boldsymbol{u}_{n+1}|_{\partial\Omega} = \mathbf{0}.
\end{cases} \qquad (26)$$

- **Step 3:** Update the pressure through the Neumann problem

$$\begin{cases}
-\nabla\cdot\left(\frac{1}{\rho_{n+1}}\nabla p_{n+1}\right) = -\nabla\cdot\left(\frac{1}{\sqrt{\rho_n\rho_{n+1}}}\nabla p_n\right) - \frac{1}{\tau}\nabla\cdot\boldsymbol{u}_{n+1}, \\
\left[\boldsymbol{n}\cdot\left(\frac{1}{\sqrt{\rho_{n+1}}}\nabla p_{n+1} - \frac{1}{\sqrt{\rho_n}}\nabla p_n\right)\right]\Big|_{\partial\Omega} = 0.
\end{cases} \qquad (27)$$

– **Step 4:** Update the end-of-step velocity $\hat{\mathbf{u}}$ *via*

$$\hat{\mathbf{u}}_{n+1} = \boldsymbol{u}_{n+1} - \frac{\tau}{\sqrt{\rho_{n+1}}}\left(\frac{1}{\sqrt{\rho_{n+1}}}\nabla p_{n+1} - \frac{1}{\sqrt{\rho_n}}\nabla p_n\right). \tag{28}$$

Notice that combining equations (27) and (28) implies, as in standard projection methods,

$$\nabla \cdot \hat{\mathbf{u}}_{n+1} = 0 \quad \text{and} \quad \boldsymbol{n} \cdot (\boldsymbol{u}_{n+1} - \hat{\mathbf{u}}_{n+1})|_{\partial\Omega} = 0. \tag{29}$$

Step 2 can be solved individually for each ith velocity component u^i_{n+1}:

$$\begin{aligned} &\frac{\rho_{n+1}}{\tau} u^i_{n+1} + \rho_{n+1}\boldsymbol{u}_n \cdot \nabla u^i_{n+1} + \frac{1}{2}\left[\nabla \cdot (\rho_{n+1}\boldsymbol{u}_n)\right] u^i_{n+1} - \nabla \cdot \left(\mu_{n+1}\nabla u^i_{n+1}\right) \\ &\quad = \frac{\sqrt{\rho_{n+1}\rho_n}}{\tau}\hat{\mathrm{u}}^i_n - \sqrt{\frac{\rho_{n+1}}{\rho_n}}\frac{\partial p_n}{\partial x_i} + \frac{\partial \boldsymbol{u}_n}{\partial x_i} \cdot \nabla \mu_{n+1} + f^i_{n+1}, \qquad i = 1, \ldots, d. \end{aligned} \tag{30}$$

This fractional-step algorithm is very simple to implement and only requires solving (in addition to the density equation) d linear scalar transport equations plus one Poisson-like problem. Moreover, up to boundary conditions, the system matrices for each of the ith velocity equations are identical, which reduces assembling efforts (see Sect. 5).

Remark 3.3. Since $\boldsymbol{n} \cdot \hat{\mathbf{u}}_{n+1} = \boldsymbol{n} \cdot \boldsymbol{u}_{n+1} = 0$ on $\partial\Omega$, we can use either $\hat{\mathbf{u}}_{n+1}$ or $\boldsymbol{u}_{n+1}$ as convective velocities for the density and momentum equations, without losing the skew-symmetry properties (14) and (15). However, implementing (28) strongly would result in a velocity $\hat{\mathbf{u}}_{n+1}$ less regular than $\boldsymbol{u}_{n+1}$, so computing its derivatives in the fully discrete case will require regularisation. In the context of finite element methods, projecting $\hat{\mathbf{u}}_{n+1}$ onto a continuous finite element space is sufficient and was the approach used in our tests.

Remark 3.4. To extend the projection step to the more general case where both Neumann and Dirichlet conditions are considered for the momentum equation, the Neumann boundary condition in (27) must be partially replaced by a Dirichlet one (see, *e.g.*, Sect. 10 in the seminal overview by Guermond *et al.* [33]).

Remark 3.5. The stability analysis of the scheme just presented will be performed independently of the approximation p_0. In fact, the stability analysis will be completely independent of the concrete approximation. A proposal for the approximation of $p(0)$ guaranteeing optimal error estimates was presented by John and Novo [34].

3.4. On second-order fractional-step schemes

Although convergence analysis is not intended in this work, we will briefly sketch the splitting error of the fractional-step scheme. Due to (28), we have

$$\frac{\sqrt{\rho_n}}{\tau}\hat{\mathbf{u}}_n = \frac{\sqrt{\rho_n}}{\tau}\boldsymbol{u}_n - \frac{1}{\sqrt{\rho_n}}\nabla p_n + \frac{1}{\sqrt{\rho_{n-1}}}\nabla p_{n-1}.$$

This can be used to eliminate the end-of-step velocity $\hat{\mathbf{u}}_n$ from the momentum step (26), which becomes

$$\begin{aligned} &\frac{\sqrt{\rho_{n+1}}}{\tau}\left(\sqrt{\rho_{n+1}}\,\boldsymbol{u}_{n+1} - \sqrt{\rho_n}\,\boldsymbol{u}_n\right) + \left(2\sqrt{\frac{\rho_{n+1}}{\rho_n}}\nabla p_n - \sqrt{\frac{\rho_{n+1}}{\rho_{n-1}}}\nabla p_{n-1}\right) \\ &\qquad + (\rho_{n+1}\nabla \boldsymbol{u}_{n+1})\boldsymbol{u}_n + \frac{1}{2}[\nabla \cdot (\rho_{n+1}\boldsymbol{u}_n)]\boldsymbol{u}_{n+1} - \nabla \cdot (\mu_{n+1}\nabla \boldsymbol{u}_{n+1}) = \nabla^\top \boldsymbol{u}_n \nabla \mu_{n+1} + \boldsymbol{f}_{n+1}. \end{aligned}$$

The resulting pressure term is in fact a second-order extrapolation:

$$\begin{aligned}2\sqrt{\frac{\rho_{n+1}}{\rho_n}}\nabla p_n - \sqrt{\frac{\rho_{n+1}}{\rho_{n-1}}}\nabla p_{n-1} &= \sqrt{\rho_{n+1}}\left[2\left(\frac{1}{\sqrt{\rho_n}}\nabla p_n\right) - \left(\frac{1}{\sqrt{\rho_{n-1}}}\nabla p_{n-1}\right)\right]\\ &= \sqrt{\rho_{n+1}}\left[\frac{1}{\sqrt{\rho_{n+1}}}\nabla p_{n+1} + \mathcal{O}(\tau^2)\right]\\ &= \nabla p_{n+1} + \mathcal{O}(\tau^2),\end{aligned}$$

where we have used the well-known formula $2\boldsymbol{v}_n - \boldsymbol{v}_{n-1} = \boldsymbol{v}_{n+1} + \mathcal{O}(\tau^2)$.

Moreover, the pressure equation (27) can be rewritten as

$$\begin{aligned}\nabla\cdot\boldsymbol{u}_{n+1} &= \tau\nabla\cdot\left[\frac{1}{\sqrt{\rho_{n+1}}}\left(\frac{1}{\sqrt{\rho_{n+1}}}\nabla p_{n+1} - \frac{1}{\sqrt{\rho_n}}\nabla p_n\right)\right]\\ &= \tau^2\nabla\cdot\left[\frac{1}{\sqrt{\rho_{n+1}}}\left(\frac{1}{\sqrt{\rho_{n+1}}}\nabla p_{n+1} - \frac{1}{\sqrt{\rho_n}}\nabla p_n\right)\Big/\tau\right]\\ &= \tau^2\nabla\cdot\left\{\frac{1}{\sqrt{\rho}}\left[\partial_t\left(\frac{1}{\sqrt{\rho}}\nabla p\right) + \mathcal{O}(\tau)\right]\right\}\Big|_{t=t_{n+1}}\\ &= \tau^2\nabla\cdot\left[\frac{1}{\sqrt{\rho}}\partial_t\left(\frac{1}{\sqrt{\rho}}\nabla p\right)\right]\Big|_{t=t_{n+1}} + \mathcal{O}(\tau^3),\end{aligned}$$

i.e., an $\mathcal{O}(\tau^2)$ perturbation (the term proportional to τ^2 dominates) of the divergence-free constraint. In other words, the fractional-step scheme itself can be reinterpreted as a first-order discretisation of the $\mathcal{O}(\tau^2)$-perturbed system

$$\begin{cases}\text{Momentum equation (10)},\\ \nabla\cdot\boldsymbol{u} - \tau^2\nabla\cdot\left[\frac{1}{\sqrt{\rho}}\partial_t\left(\frac{1}{\sqrt{\rho}}\nabla p\right)\right] = 0.\end{cases} \tag{31}$$

Therefore, in principle, the fractional-step algorithm presented above could be extended to second order by combining, for instance, BDF2 and second-order extrapolations. However, while several such schemes have been proved convergent for homogeneous flows [33,35,36], the situation is much more challenging for variable density, for which there still seems to be no provably stable second-order projection method [14]. In this context, we shall presently refrain from formally proposing an IMEX fractional-step scheme of second order.

Remark 3.6. For constant density, the perturbation to the incompressibility constraint would reduce to the well-known term $-\tau^2\partial_t\Delta p$ appearing in the classical incremental pressure-correction method [33].

4. Stability analysis

We will next derive temporal stability proofs for each of the three schemes proposed herein (a reader not so interested in the theory may skip to Sect. 5, where we discuss implementation). As usual for the analysis, we assume homogeneous Dirichlet data: $\boldsymbol{u}_{n+1} = \boldsymbol{0}$ on $\partial\Omega$ for all t_{n+1}. In the proofs, C denotes a generic positive constant depending only on initial conditions, on problem data and on τ, and which does not grow with decreasing τ ($\partial_\tau C \geq 0$ for all $\tau > 0$). Although we will not discuss spatial stability, the theory presented in this section holds, *e.g.*, for standard H^1-conforming finite element spaces. Before analysing the velocity, we state the stability of ρ.

Lemma 4.1 (Density stability)**.** *For any time-step size $\tau = T/N$, the BDF schemes (18) and (19) yield, respectively,*

$$\|\rho_N\|^2 + \sum_{n=1}^{N}\|\delta\rho_n\|^2 = \|\rho_0\|^2$$

and

$$\|\rho_N\|^2 + \|\rho_N^\star\|^2 + \sum_{n=1}^{N} \|\delta^2 \rho_n\|^2 = \|\rho_1\|^2 + \|\rho_1^\star\|^2.$$

Proof. These classical results follow immediately from the skew-symmetry (14) and the identities (12) and (13). $\square$

Remark 4.1. The following stability estimates assume that at each time step $t = t_{n+1}$, the forcing term satisfies $\boldsymbol{f}_{n+1} \in [H^{-1}(\Omega)]^d$. Modified estimates considering $\boldsymbol{f} \in [L^2(Q)]^d$ can also be derived, as done in our recent work [22].

4.1. First-order coupled scheme

For the first-order coupled IMEX scheme, we will prove the following stability estimate.

Theorem 4.2 (Stability of the first-order coupled scheme)**.** *For any time-step size $\tau = T/N$, $N \geq 1$, the IMEX scheme ((18), (21), (22)) satisfies the stability estimate*

$$\begin{aligned} \|\sqrt{\rho_N}\, \boldsymbol{u}_N\|^2 + \tau\varepsilon \|\sqrt{\mu_N}\, \nabla \boldsymbol{u}_N\|^2 + \tau\,(2 - \epsilon - \varepsilon) \sum_{n=1}^{N} \|\sqrt{\mu_n}\, \nabla \boldsymbol{u}_n\|^2 \\ \leq \left(C + \sum_{n=1}^{N} \frac{\tau}{\epsilon \mu_{\min}} \|\boldsymbol{f}_n\|_{-1}^2 \right) \exp\left(\frac{T\, \|\nabla \mu\|_\infty^2}{\varepsilon \varrho_{\min} \mu_{\min}} \right), \end{aligned} \tag{32}$$

where ε, ϵ are two positive constants such that $\varepsilon + \epsilon \leq 2$.

Proof. We start by testing equations (21) and (22) with $2\tau \boldsymbol{u}_{n+1}$ and $2\tau p_{n+1}$, respectively, adding the two results together and using integration by parts, which yields

$$\|\boldsymbol{U}_{n+1}\|^2 - \|\boldsymbol{U}_n\|^2 + \|\delta \boldsymbol{U}_{n+1}\|^2 + 2\tau \left\|\sqrt{\mu_{n+1}}\, \nabla \boldsymbol{u}_{n+1}\right\|^2 = 2\tau \left(\nabla^\top \boldsymbol{u}_n \nabla \mu_{n+1}, \boldsymbol{u}_{n+1}\right) + 2\tau \left\langle \boldsymbol{f}_{n+1}, \boldsymbol{u}_{n+1} \right\rangle, \tag{33}$$

where the convective terms vanished due to (12). We must bound both terms on the right-hand side of (33). Using Hölder's and Young's inequalities, we get

$$\begin{aligned} 2\tau \left(\nabla^\top \boldsymbol{u}_n \nabla \mu_{n+1}, \boldsymbol{u}_{n+1}\right) &= 2\tau \left(\frac{1}{\sqrt{\rho_{n+1}}} \nabla^\top \boldsymbol{u}_n \nabla \mu_{n+1}, \boldsymbol{U}_{n+1} \right) \\ &= 2\tau \left(\frac{1}{\sqrt{\rho_{n+1}}} \nabla^\top \boldsymbol{u}_n \nabla \mu_{n+1}, \delta \boldsymbol{U}_{n+1} + \boldsymbol{U}_n \right) \\ &\leq 2\tau \frac{\|\nabla \mu\|_\infty}{\sqrt{\varrho_{\min}}} \|\nabla \boldsymbol{u}_n\|\, \|\delta \boldsymbol{U}_{n+1}\| + 2\tau \frac{\|\nabla \mu\|_\infty}{\sqrt{\varrho_{\min}}} \|\nabla \boldsymbol{u}_n\|\, \|\boldsymbol{U}_n\| \\ &\leq \|\delta \boldsymbol{U}_{n+1}\|^2 + \tau^2 \frac{\|\nabla \mu\|_\infty^2}{\varrho_{\min}} \|\nabla \boldsymbol{u}_n\|^2 + \tau\varepsilon\mu_{\min} \|\nabla \boldsymbol{u}_n\|^2 + \frac{\tau \|\nabla \mu\|_\infty^2}{\varepsilon \varrho_{\min} \mu_{\min}} \|\boldsymbol{U}_n\|^2 \\ &= \|\delta \boldsymbol{U}_{n+1}\|^2 + \tau\varepsilon\mu_{\min} \|\nabla \boldsymbol{u}_n\|^2 + \frac{\tau \|\nabla \mu\|_\infty^2}{\varepsilon \varrho_{\min} \mu_{\min}} \left(\|\boldsymbol{U}_n\|^2 + \tau\varepsilon\mu_{\min} \|\nabla \boldsymbol{u}_n\|^2 \right) \\ &\leq \|\delta \boldsymbol{U}_{n+1}\|^2 + \tau\varepsilon \|\sqrt{\mu_n}\, \nabla \boldsymbol{u}_n\|^2 + \frac{\tau \|\nabla \mu\|_\infty^2}{\varepsilon \varrho_{\min} \mu_{\min}} \left(\|\boldsymbol{U}_n\|^2 + \tau\varepsilon \|\sqrt{\mu_n}\, \nabla \boldsymbol{u}_n\|^2 \right), \end{aligned} \tag{34}$$

and

$$
\begin{aligned}
2\tau\langle \boldsymbol{f}_{n+1}, \boldsymbol{u}_{n+1}\rangle &\leq 2\tau\|\boldsymbol{f}_{n+1}\|_{-1}\|\nabla \boldsymbol{u}_{n+1}\| \\
&\leq \frac{\tau}{\epsilon\mu_{\min}}\|\boldsymbol{f}_{n+1}\|_{-1}^2 + \tau\epsilon\mu_{\min}\|\nabla \boldsymbol{u}_{n+1}\|^2 \\
&\leq \frac{\tau}{\epsilon\mu_{\min}}\|\boldsymbol{f}_{n+1}\|_{-1}^2 + \tau\epsilon\|\sqrt{\mu_{n+1}}\,\nabla \boldsymbol{u}_{n+1}\|^2,
\end{aligned} \tag{35}
$$

for arbitrary $\varepsilon, \epsilon > 0$. Inserting (34) and (35) in (33) gives

$$
\begin{aligned}
&\|\boldsymbol{U}_{n+1}\|^2 - \|\boldsymbol{U}_n\|^2 + \tau(2-\epsilon)\big\|\sqrt{\mu_{n+1}}\,\nabla \boldsymbol{u}_{n+1}\big\|^2 \\
&\quad\leq \tau\varepsilon\|\sqrt{\mu_n}\,\nabla \boldsymbol{u}_n\|^2 + \frac{\tau\|\nabla\mu\|_\infty^2}{\varepsilon\varrho_{\min}\mu_{\min}}\left(\|\boldsymbol{U}_n\|^2 + \tau\varepsilon\,\|\sqrt{\mu_n}\,\nabla \boldsymbol{u}_n\|^2\right) + \frac{\tau}{\epsilon\mu_{\min}}\,\big\|\boldsymbol{f}_{n+1}\big\|_{-1}^2.
\end{aligned}
$$

Adding up from $n = 0$ to $n = N-1$ yields

$$
\begin{aligned}
&\|\boldsymbol{U}_N\|^2 + \tau\varepsilon\|\sqrt{\mu_N}\,\nabla \boldsymbol{u}_N\|^2 + \tau(2-\epsilon-\varepsilon)\sum_{n=1}^{N}\big\|\sqrt{\mu_n}\,\nabla \boldsymbol{u}_n\big\|^2 \\
&\quad\leq \|\boldsymbol{U}_0\|^2 + \tau\varepsilon\,\|\sqrt{\mu_0}\,\nabla \boldsymbol{u}_0\|^2 + \frac{\tau\|\nabla\mu\|_\infty^2}{\varepsilon\varrho_{\min}\mu_{\min}}\sum_{n=0}^{N-1}\left(\|\boldsymbol{U}_n\|^2 + \tau\varepsilon\,\|\sqrt{\mu_n}\,\nabla \boldsymbol{u}_n\|^2\right) + \sum_{n=1}^{N}\frac{\tau}{\epsilon\mu_{\min}}\,\|\boldsymbol{f}_n\|_{-1}^2.
\end{aligned}
$$

Estimate (32) now follows directly from the Gronwall lemma, with $a_n = \|\boldsymbol{U}_n\|^2 + \tau\varepsilon\|\sqrt{\mu_n}\,\nabla \boldsymbol{u}_n\|^2$, $b_n = \tau(2 - \epsilon - \varepsilon)\big\|\sqrt{\mu_n}\,\nabla \boldsymbol{u}_n\big\|^2$ and $c_n = \frac{\tau}{\epsilon\mu_{\min}}\|\boldsymbol{f}_n\|_{-1}^2$. □

4.2. Second-order coupled scheme

Unlike the scheme just analysed, the second-order version is not self-starting, since ρ_{n-1} and $\boldsymbol{u}_{n-1}$ are not defined at the first time step ($n = 0$). The simplest approach is to start with the first-order method ((18), (21), (22)). From the second time step onwards we use the second-order scheme, for which we will prove the following stability result.

Theorem 4.3 (Stability of the second-order coupled scheme)**.** *For any time-step size $\tau = T/N$, $N \geq 2$, the IMEX scheme ((19), (23), (24)) satisfies the stability estimate*

$$
\begin{aligned}
&\|\sqrt{\rho_N}\,\boldsymbol{u}_N\|^2 + \big\|2\sqrt{\rho_N}\,\boldsymbol{u}_N - \sqrt{\rho_{N-1}}\,\boldsymbol{u}_{N-1}\big\|^2 + 40\tau\varepsilon\big\|\sqrt{\mu_N}\,\nabla \boldsymbol{u}_N\big\|^2 \\
&\quad + 4\tau\sum_{n=1}^{N}\left[(1-\epsilon-10\varepsilon)\big\|\sqrt{\mu_n}\,\nabla \boldsymbol{u}_n\big\|^2 + \varepsilon\mu_{\min}\big\|2\nabla \boldsymbol{u}_{n-1} + \nabla \boldsymbol{u}_{n-2}\big\|^2\right] \\
&\quad \leq \left(\tilde{C} + \sum_{n=1}^{N}\frac{\tau}{\epsilon\mu_{\min}}\|\boldsymbol{f}_n\|_{-1}^2\right)\exp\left(\frac{T\|\nabla\mu\|_\infty^2}{\varepsilon\varrho_{\min}\mu_{\min}}\right),
\end{aligned} \tag{36}
$$

where ε, ϵ are two positive constants such that $10\varepsilon + \epsilon \leq 1$.

Proof. We start by testing equations (23) and (24) with $4\tau\boldsymbol{u}_{n+1}$ and $4\tau p_{n+1}$, respectively, and adding those results, so that

$$
\begin{aligned}
&\|\boldsymbol{U}_{n+1}\|^2 + \big\|\boldsymbol{U}_{n+1}^\star\big\|^2 - \|\boldsymbol{U}_n\|^2 - \|\boldsymbol{U}_n^\star\|^2 + \big\|\delta^2\boldsymbol{U}_{n+1}\big\|^2 + 4\tau\,\big\|\sqrt{\mu_{n+1}}\,\nabla \boldsymbol{u}_{n+1}\big\|^2 \\
&\quad = 4\tau\left(\nabla^\top \boldsymbol{u}_n^\star\nabla\mu_{n+1}, \boldsymbol{u}_{n+1}\right) + 4\tau\left\langle \boldsymbol{f}_{n+1}, \boldsymbol{u}_{n+1}\right\rangle.
\end{aligned} \tag{37}
$$

The last term on the right-hand side is estimated as

$$4\tau \left\langle \boldsymbol{f}_{n+1}, \boldsymbol{u}_{n+1} \right\rangle \leq \frac{\tau}{\epsilon \mu_{\min}} \left\| \boldsymbol{f}_{n+1} \right\|_{-1}^2 + 4\tau\epsilon \left\| \sqrt{\mu_{n+1}}\, \nabla \boldsymbol{u}_{n+1} \right\|^2 . \tag{38}$$

For the remaining term we have

$$\begin{aligned}
4\tau \left(\nabla^\top \boldsymbol{u}_n^\star \nabla \mu_{n+1}, \boldsymbol{u}_{n+1} \right) &= 4\tau \left(\frac{1}{\sqrt{\rho_{n+1}}} \nabla^\top \boldsymbol{u}_n^\star \nabla \mu_{n+1}, \boldsymbol{U}_{n+1} \right) \\
&= 4\tau \left(\frac{1}{\sqrt{\rho_{n+1}}} \nabla^\top \boldsymbol{u}_n^\star \nabla \mu_{n+1}, \delta^2 \boldsymbol{U}_{n+1} + \boldsymbol{U}_n^\star \right) \\
&\leq 4\tau \frac{\|\nabla \mu\|_\infty}{\sqrt{\varrho_{\min}}} \|\nabla \boldsymbol{u}_n^\star\| \left\| \delta^2 \boldsymbol{U}_{n+1} \right\| + 4\tau \frac{\|\nabla \mu\|_\infty}{\sqrt{\varrho_{\min}}} \|\nabla \boldsymbol{u}_n^\star\| \, \|\boldsymbol{U}_n^\star\| \\
&\leq \left\| \delta^2 \boldsymbol{U}_{n+1} \right\|^2 + 4\tau^2 \frac{\|\nabla \mu\|_\infty^2}{\varrho_{\min}} \|\nabla \boldsymbol{u}_n^\star\|^2 + 4\tau\varepsilon\mu_{\min} \|\nabla \boldsymbol{u}_n^\star\|^2 + \frac{\tau \|\nabla \mu\|_\infty^2}{\varepsilon \varrho_{\min} \mu_{\min}} \|\boldsymbol{U}_n^\star\|^2 .
\end{aligned}$$

For the viscous terms above, we use

$$\begin{aligned}
\mu_{\min} \|\nabla \boldsymbol{u}_n^\star\|^2 &= \mu_{\min} \|2\nabla \boldsymbol{u}_n - \nabla \boldsymbol{u}_{n-1}\|^2 \\
&= \mu_{\min} \left(2 \|2\nabla \boldsymbol{u}_n\|^2 + 2 \|\nabla \boldsymbol{u}_{n-1}\|^2 - \|2\nabla \boldsymbol{u}_n + \nabla \boldsymbol{u}_{n-1}\|^2 \right) \\
&\leq 2 \left(\|2\sqrt{\mu_n}\, \nabla \boldsymbol{u}_n\|^2 + \left\| \sqrt{\mu_{n-1}}\, \nabla \boldsymbol{u}_{n-1} \right\|^2 \right) - \mu_{\min} \|2\nabla \boldsymbol{u}_n + \nabla \boldsymbol{u}_{n-1}\|^2 \\
&\leq 8 \|\sqrt{\mu_n}\, \nabla \boldsymbol{u}_n\|^2 + 2 \left\| \sqrt{\mu_{n-1}}\, \nabla \boldsymbol{u}_{n-1} \right\|^2 ,
\end{aligned}$$

so that

$$\begin{aligned}
&4\tau \left(\nabla^\top \boldsymbol{u}_n^\star \nabla \mu_{n+1}, \boldsymbol{u}_{n+1} \right) \\
&\quad \leq \left\| \delta^2 \boldsymbol{U}_{n+1} \right\|^2 + \tau\varepsilon \left(32 \left\| \sqrt{\mu_n}\, \nabla \boldsymbol{u}_n \right\|^2 + 8 \left\| \sqrt{\mu_{n-1}}\, \nabla \boldsymbol{u}_{n-1} \right\|^2 - 4\mu_{\min} \left\| 2\nabla \boldsymbol{u}_n + \nabla \boldsymbol{u}_{n-1} \right\|^2 \right) \\
&\qquad + \frac{\tau \|\nabla \mu\|_\infty^2}{\varepsilon \varrho_{\min} \mu_{\min}} \left(\|\boldsymbol{U}_n^\star\|^2 + 32\varepsilon\tau \|\sqrt{\mu_n}\, \nabla \boldsymbol{u}_n\|^2 + 8\varepsilon\tau \left\| \sqrt{\mu_{n-1}}\, \nabla \boldsymbol{u}_{n-1} \right\|^2 \right) .
\end{aligned} \tag{39}$$

Combining equations (37)–(39) yields

$$\begin{aligned}
&\|\boldsymbol{U}_{n+1}\|^2 + \left\| \boldsymbol{U}_{n+1}^\star \right\|^2 + 4\tau(1-\epsilon) \left\| \sqrt{\mu_{n+1}}\, \nabla \boldsymbol{u}_{n+1} \right\|^2 + 4\tau\varepsilon\mu_{\min} \|2\nabla \boldsymbol{u}_n + \nabla \boldsymbol{u}_{n-1}\|^2 \\
&\quad \leq \|\boldsymbol{U}_n\|^2 + \|\boldsymbol{U}_n^\star\|^2 + \frac{\tau}{\epsilon \mu_{\min}} \left\| \boldsymbol{f}_{n+1} \right\|_{-1}^2 + 4\tau\varepsilon \left(8 \|\sqrt{\mu_n}\, \nabla \boldsymbol{u}_n\|^2 + 2 \left\| \sqrt{\mu_{n-1}}\, \nabla \boldsymbol{u}_{n-1} \right\|^2 \right) \\
&\qquad + \frac{\tau \|\nabla \mu\|_\infty^2}{\varepsilon \varrho_{\min} \mu_{\min}} \left(\|\boldsymbol{U}_n^\star\|^2 + 32\varepsilon\tau \|\sqrt{\mu_n}\, \nabla \boldsymbol{u}_n\|^2 + 8\varepsilon\tau \left\| \sqrt{\mu_{n-1}}\, \nabla \boldsymbol{u}_{n-1} \right\|^2 \right) .
\end{aligned} \tag{40}$$

We will now sum (40) from $n = 1$ to $N - 1$. For the viscous term, we have that

$$\begin{aligned}
&\sum_{n=1}^{N-1} \left[(1-\epsilon) \left\| \sqrt{\mu_{n+1}}\, \nabla \boldsymbol{u}_{n+1} \right\|^2 - 8\varepsilon \|\sqrt{\mu_n}\, \nabla \boldsymbol{u}_n\|^2 - 2\varepsilon \|\sqrt{\mu_{n-1}}\, \nabla \boldsymbol{u}_{n-1}\|^2 \right] \\
&\quad = 10\varepsilon \left(\|\sqrt{\mu_N}\, \nabla \boldsymbol{u}_N\|^2 - \|\sqrt{\mu_1}\, \nabla \boldsymbol{u}_1\|^2 \right) + 2\varepsilon \left(\left\| \sqrt{\mu_{N-1}}\, \nabla \boldsymbol{u}_{N-1} \right\|^2 - \|\sqrt{\mu_0}\, \nabla \boldsymbol{u}_0\|^2 \right) \\
&\qquad + (1-\epsilon-10\varepsilon) \sum_{n=1}^{N-1} \left\| \sqrt{\mu_{n+1}}\, \nabla \boldsymbol{u}_{n+1} \right\|^2 \\
&\quad \geq 10\varepsilon \|\sqrt{\mu_N}\, \nabla \boldsymbol{u}_N\|^2 - \varepsilon \left(10 \|\sqrt{\mu_1}\, \nabla \boldsymbol{u}_1\|^2 + 2 \|\sqrt{\mu_0}\, \nabla \boldsymbol{u}_0\|^2 \right) + (1-\epsilon-10\varepsilon) \sum_{n=1}^{N-1} \left\| \sqrt{\mu_{n+1}}\, \nabla \boldsymbol{u}_{n+1} \right\|^2 ,
\end{aligned}$$

hence

$$
\begin{aligned}
&\|\boldsymbol{U}_N\|^2 + \|\boldsymbol{U}_N^\star\|^2 + 40\varepsilon\tau \left\|\sqrt{\mu_N}\,\nabla \boldsymbol{u}_N\right\|^2 \\
&\qquad + 4\tau \sum_{n=2}^{N} \left[(1-\epsilon-10\varepsilon) \left\|\sqrt{\mu_n}\,\nabla \boldsymbol{u}_n\right\|^2 + \varepsilon\mu_{\min} \left\|2\nabla \boldsymbol{u}_{n-1} + \nabla \boldsymbol{u}_{n-2}\right\|^2 \right] \\
&\qquad \leq \|\boldsymbol{U}_1\|^2 + \|\boldsymbol{U}_1^\star\|^2 + 4\tau\varepsilon \left(10 \left\|\sqrt{\mu_1}\,\nabla \boldsymbol{u}_1\right\|^2 + 2\left\|\sqrt{\mu_0}\,\nabla \boldsymbol{u}_0\right\|^2 \right) + \frac{\tau}{\epsilon\mu_{\min}} \sum_{n=2}^{N} \|\boldsymbol{f}_n\|_{-1}^2 \\
&\qquad\quad + \frac{\tau\|\nabla\mu\|_\infty^2}{\varepsilon\varrho_{\min}\mu_{\min}} \sum_{n=1}^{N-1} \left(\|\boldsymbol{U}_n^\star\|^2 + 32\varepsilon\tau \left\|\sqrt{\mu_n}\,\nabla \boldsymbol{u}_n\right\|^2 + 8\varepsilon\tau \left\|\sqrt{\mu_{n-1}}\,\nabla \boldsymbol{u}_{n-1}\right\|^2 \right) \\
&\qquad \leq C + \frac{\tau\|\nabla\mu\|_\infty^2}{\varepsilon\varrho_{\min}\mu_{\min}} \sum_{n=1}^{N-1} \left(\|\boldsymbol{U}_n^\star\|^2 + 40\varepsilon\tau \|\sqrt{\mu_n}\,\nabla \boldsymbol{u}_n\|^2 \right) + \frac{\tau}{\epsilon\mu_{\min}} \sum_{n=2}^{N} \|\boldsymbol{f}_n\|_{-1}^2 \\
&\qquad \leq \tilde{C} + \frac{\tau\|\nabla\mu\|_\infty^2}{\varepsilon\varrho_{\min}\mu_{\min}} \sum_{n=1}^{N-1} \left(\|\boldsymbol{U}_n\|^2 + \|\boldsymbol{U}_n^\star\|^2 + 40\varepsilon\tau \left\|\sqrt{\mu_n}\,\nabla \boldsymbol{u}_n\right\|^2 \right) + \frac{\tau}{\epsilon\mu_{\min}} \sum_{n=1}^{N} \|\boldsymbol{f}_n\|_{-1}^2,
\end{aligned}
\tag{41}
$$

from which stability follows provided that $\epsilon + 10\varepsilon \leq 1$, using the Gronwall inequality. □

Remark 4.2. In (41), we were able to incorporate the contributions from the first time step into the finite constant $\tilde{C}$ because of the already proven stability of the first-order scheme, which is used for initialisation.

4.3. Fractional-step scheme

We will now prove that our fractional-step IMEX method is also unconditionally stable.

Theorem 4.4 (Stability of the fractional-step IMEX scheme)**.** *For any time-step size $\tau = T/N$, $N \geq 1$, the IMEX scheme (26)–(28) satisfies the stability estimate*

$$
\begin{aligned}
&\left\|\sqrt{\rho_N}\,\hat{\mathbf{u}}_N\right\|^2 + \tau\varepsilon \left\|\sqrt{\mu_N}\,\nabla \boldsymbol{u}_N\right\|^2 + \tau^2 \left\| \frac{1}{\sqrt{\rho_N}} \nabla p_N \right\|^2 + (2-\epsilon-\varepsilon)\,\tau \sum_{n=1}^{N} \left\|\sqrt{\mu_n}\,\nabla \boldsymbol{u}_n\right\|^2 \\
&\qquad \leq \left(C + \sum_{n=1}^{N} \frac{\tau}{\epsilon\mu_{\min}} \|\boldsymbol{f}_n\|_{-1}^2 \right) \exp\left(\frac{T\|\nabla\mu\|_\infty^2}{\varepsilon\varrho_{\min}\mu_{\min}} \right),
\end{aligned}
\tag{42}
$$

where ε, ϵ are two positive constants such that $\varepsilon + \epsilon \leq 2$.

Proof. Let us test the first equation in (26) against $2\tau \boldsymbol{u}_{n+1}$, so that

$$
\begin{aligned}
&\|\boldsymbol{U}_{n+1}\|^2 - \left\|\hat{\mathbf{U}}_n\right\|^2 + \left\|\boldsymbol{U}_{n+1} - \hat{\mathbf{U}}_n\right\|^2 + 2\tau \left\|\sqrt{\mu_{n+1}}\,\nabla \boldsymbol{u}_{n+1}\right\|^2 \\
&\qquad = 2\tau \left(\nabla^\top \boldsymbol{u}_n \nabla\mu_{n+1}, \boldsymbol{u}_{n+1}\right) + 2\tau \left\langle \boldsymbol{f}_{n+1}, \boldsymbol{u}_{n+1} \right\rangle - 2\tau \left(\chi_n \nabla p_n, \boldsymbol{U}_{n+1}\right),
\end{aligned}
\tag{43}
$$

introducing the short-hand notation $\chi_n := 1/\sqrt{\rho_n}$ and $\hat{\mathbf{U}}_n := \sqrt{\rho_n}\,\hat{\mathbf{u}}_n$. Then, testing (27) with $2\tau p_{n+1}$ gives

$$
\begin{aligned}
\tau \left(\|\chi_{n+1}\nabla p_{n+1}\|^2 - \|\chi_n \nabla p_n\|^2 + \|\chi_{n+1}\nabla p_{n+1} - \chi_n\nabla p_n\|^2 \right) &= 2\left(-\nabla\cdot \boldsymbol{u}_{n+1}, p_{n+1}\right) \\
&= 2\left(\nabla\cdot\hat{\mathbf{u}}_{n+1} - \nabla\cdot \boldsymbol{u}_{n+1}, p_{n+1}\right) \\
&= 2\left(\boldsymbol{u}_{n+1} - \hat{\mathbf{u}}_{n+1}, \nabla p_{n+1}\right) \\
&= 2\left(\boldsymbol{U}_{n+1} - \hat{\mathbf{U}}_{n+1}, \chi_{n+1}\nabla p_{n+1}\right),
\end{aligned}
$$

where we have used (29). This, combined with equation (28), yields

$$\tau^2 \left\|\chi_{n+1}\nabla p_{n+1}\right\|^2 - \tau^2 \left\|\chi_n \nabla p_n\right\|^2 + \left\|\boldsymbol{U}_{n+1} - \hat{\mathbf{U}}_n\right\|^2 = 2\tau\left(\boldsymbol{U}_{n+1} - \hat{\mathbf{U}}_{n+1}, \chi_{n+1}\nabla p_{n+1}\right). \tag{44}$$

We now test equation (28) against $2\rho_{n+1}\hat{\mathbf{u}}_{n+1}$, resulting in

$$\begin{aligned} \left\|\hat{\mathbf{U}}_{n+1}\right\|^2 - \left\|\boldsymbol{U}_{n+1}\right\|^2 + \left\|\boldsymbol{U}_{n+1} - \hat{\mathbf{U}}_{n+1}\right\|^2 &= -2\tau\left(\chi_{n+1}\nabla p_{n+1} - \chi_n\nabla p_n, \hat{\mathbf{U}}_{n+1}\right) \\ &= 2\tau\left(\chi_n\nabla p_n, \hat{\mathbf{U}}_{n+1}\right) - 2\tau\left(\nabla p_{n+1}, \hat{\mathbf{u}}_{n+1}\right) \\ &= 2\tau\left(\chi_n\nabla p_n, \hat{\mathbf{U}}_{n+1}\right), \end{aligned} \tag{45}$$

again due to (29). So, adding equations (43)–(45) yields

$$\begin{aligned} &\left\|\hat{\mathbf{U}}_{n+1}\right\|^2 - \left\|\hat{\mathbf{U}}_n\right\|^2 + \left\|\boldsymbol{U}_{n+1} - \hat{\mathbf{U}}_n\right\|^2 + 2\tau\left\|\sqrt{\mu_{n+1}}\,\nabla\boldsymbol{u}_{n+1}\right\|^2 + \tau^2\left(\left\|\chi_{n+1}\nabla p_{n+1}\right\|^2 - \left\|\chi_n\nabla p_n\right\|^2\right) \\ &\quad = 2\tau\left(\nabla^\top\boldsymbol{u}_n\nabla\mu_n, \boldsymbol{u}_{n+1}\right) + 2\tau\left\langle \boldsymbol{f}_{n+1}, \boldsymbol{u}_{n+1}\right\rangle \\ &\qquad + 2\tau\left(\chi_{n+1}\nabla p_{n+1} - \chi_n\nabla p_n, \boldsymbol{U}_{n+1} - \hat{\mathbf{U}}_{n+1}\right) - 2\left\|\boldsymbol{U}_{n+1} - \hat{\mathbf{U}}_{n+1}\right\|^2, \end{aligned} \tag{46}$$

where the last two terms on the right-hand side cancel out, since

$$\tau\left(\chi_{n+1}\nabla p_{n+1} - \chi_n\nabla p_n, \boldsymbol{U}_{n+1} - \hat{\mathbf{U}}_{n+1}\right) = \left\|\boldsymbol{U}_{n+1} - \hat{\mathbf{U}}_{n+1}\right\|^2,$$

by construction (of the projected velocity $\hat{\mathbf{u}}_{n+1}$, see Eq. (28)).

For the explicit part of the viscous term in (46) we write, similarly as in (34),

$$\begin{aligned} 2\tau\left(\nabla^\top\boldsymbol{u}_n\nabla\mu_{n+1}, \boldsymbol{u}_{n+1}\right) &= 2\tau\left(\frac{1}{\sqrt{\rho_{n+1}}}\nabla^\top\boldsymbol{u}_n\nabla\mu_{n+1}, \boldsymbol{U}_{n+1}\right) \\ &= 2\tau\left(\frac{1}{\sqrt{\rho_{n+1}}}\nabla^\top\boldsymbol{u}_n\nabla\mu_{n+1}, \boldsymbol{U}_{n+1} - \hat{\mathbf{U}}_n + \hat{\mathbf{U}}_n\right) \\ &\le 2\tau\frac{\|\nabla\mu\|_\infty}{\sqrt{\varrho_{\min}}}\left\|\nabla\boldsymbol{u}_n\right\|\left\|\boldsymbol{U}_{n+1} - \hat{\mathbf{U}}_n\right\| + 2\tau\frac{\|\nabla\mu\|_\infty}{\sqrt{\varrho_{\min}}}\left\|\nabla\boldsymbol{u}_n\right\|\left\|\hat{\mathbf{U}}_n\right\| \\ &\le \left\|\boldsymbol{U}_{n+1} - \hat{\mathbf{U}}_n\right\|^2 + \tau\varepsilon\left\|\sqrt{\mu_n}\,\nabla\boldsymbol{u}_n\right\|^2 + \frac{\tau\left\|\nabla\mu\right\|_\infty^2}{\varepsilon\varrho_{\min}\mu_{\min}}\left(\left\|\hat{\mathbf{U}}_n\right\|^2 + \tau\varepsilon\left\|\sqrt{\mu_n}\,\nabla\boldsymbol{u}_n\right\|^2\right). \end{aligned} \tag{47}$$

Finally, by estimating the forcing term as we did for the coupled scheme and combining that estimate with (46) and (47), we obtain

$$\begin{aligned} &\left\|\hat{\mathbf{U}}_{n+1}\right\|^2 - \left\|\hat{\mathbf{U}}_n\right\|^2 + \tau^2\left(\left\|\chi_{n+1}\nabla p_{n+1}\right\|^2 - \left\|\chi_n\nabla p_n\right\|^2\right) + (2-\epsilon)\tau\left\|\sqrt{\mu_{n+1}}\,\nabla\boldsymbol{u}_{n+1}\right\|^2 \\ &\quad \le \varepsilon\tau\left\|\sqrt{\mu_n}\,\nabla\boldsymbol{u}_n\right\|^2 + \frac{\tau\|\nabla\mu\|_\infty^2}{\varepsilon\varrho_{\min}\mu_{\min}}\left(\left\|\hat{\mathbf{U}}_n\right\|^2 + \tau\varepsilon\left\|\sqrt{\mu_n}\,\nabla\boldsymbol{u}_n\right\|^2\right) + \frac{\tau}{\epsilon\mu_{\min}}\left\|\boldsymbol{f}_{n+1}\right\|_{-1}^2 \\ &\quad \le \varepsilon\tau\left\|\sqrt{\mu_n}\,\nabla\boldsymbol{u}_n\right\|^2 + \frac{\tau\|\nabla\mu\|_\infty^2}{\varepsilon\varrho_{\min}\mu_{\min}}\left(\left\|\hat{\mathbf{U}}_n\right\|^2 + \tau^2\left\|\chi_n\nabla p_n\right\|^2 + \tau\varepsilon\left\|\sqrt{\mu_n}\,\nabla\boldsymbol{u}_n\right\|^2\right) + \frac{\tau}{\epsilon\mu_{\min}}\left\|\boldsymbol{f}_{n+1}\right\|_{-1}^2. \end{aligned}$$

Adding from $n = 0$ to $n = N - 1$ and using the Gronwall lemma completes the proof. ☐

4.4. On the unique solvability of the schemes

We have not yet discussed the well-posedness of our schemes, *i.e.*, whether each time step indeed produces a unique pair $(\boldsymbol{u}_{n+1}, p_{n+1})$. To address this, we will focus on the fractional-step scheme, since the analysis of the coupled variants is similar but more classical. Let us start by rewriting (26)–(28) as the weak problem to find $(\boldsymbol{u}_{n+1}, \hat{\mathbf{u}}_{n+1}, p_{n+1}) \in X \times Y \times Z$ such that

$$A\left((\boldsymbol{u}_{n+1}, \hat{\mathbf{u}}_{n+1}, p_{n+1}), (\boldsymbol{v}, \hat{\mathbf{v}}, q)\right) = f(\boldsymbol{v}, \hat{\mathbf{v}}, q) \tag{48}$$

for all $(\boldsymbol{v}, \hat{\mathbf{v}}, q) \in X \times Y \times Z$, where $X = [H_0^1(\Omega)]^d$, $Y = [L^2(\Omega)]^d$, $Z = L_0^2(\Omega) \cap H^1(\Omega)$, and the bilinear and linear forms are

$$\begin{aligned} &A\left((\boldsymbol{u}_{n+1}, \hat{\mathbf{u}}_{n+1}, p_{n+1}), (\boldsymbol{v}, \hat{\mathbf{v}}, q)\right) \\ &\quad := \left(\frac{\rho_{n+1}}{\tau}\boldsymbol{u}_{n+1} + (\rho_{n+1}\nabla \boldsymbol{u}_{n+1})\,\boldsymbol{u}_n + \frac{1}{2}\left[\nabla\cdot(\rho_{n+1}\boldsymbol{u}_n)\right]\boldsymbol{u}_{n+1}, \boldsymbol{v}\right) + (\mu_{n+1}\nabla\boldsymbol{u}_{n+1}, \nabla\boldsymbol{v}) \\ &\qquad + \tau\left(\frac{1}{\rho_{n+1}}\nabla p_{n+1}, \nabla q\right) + (\nabla\cdot\boldsymbol{u}_{n+1}, q) + \frac{1}{\tau}\left(\hat{\mathbf{u}}_{n+1} - \boldsymbol{u}_{n+1}, \rho_{n+1}\hat{\mathbf{v}}\right) + (\nabla p_{n+1}, \hat{\mathbf{v}}) \end{aligned} \tag{49}$$

and

$$\begin{aligned} f(\boldsymbol{v}, \hat{\mathbf{v}}, q) = &\left(\frac{\sqrt{\rho_{n+1}\rho_n}}{\tau}\hat{\mathbf{u}}_n - \sqrt{\frac{\rho_{n+1}}{\rho_n}}\nabla p_n + \nabla^\top\boldsymbol{u}_n\nabla\mu_{n+1}, \boldsymbol{v}\right) + \langle \boldsymbol{f}_{n+1}, \boldsymbol{v}\rangle \\ &+ \tau\left(\frac{1}{\sqrt{\rho_{n+1}}}\nabla p_n, \frac{1}{\sqrt{\rho_n}}\nabla q\right) + \left(\sqrt{\frac{\rho_{n+1}}{\rho_n}}\nabla p_n, \hat{\mathbf{v}}\right). \end{aligned} \tag{50}$$

We will prove the unique solvability of (48) by showing that the linear form f is bounded and the bilinear form A is coercive with respect to the norm

$$|\!|\!|(\boldsymbol{v}, \hat{\mathbf{v}}, q)|\!|\!| := \left(\frac{1}{\tau}\left\|\sqrt{\rho_{n+1}}\,\hat{\mathbf{v}}\right\|^2 + \frac{1}{\tau}\left\|\sqrt{\rho_{n+1}}\,\boldsymbol{v}\right\|^2 + 2\left\|\sqrt{\mu_{n+1}}\,\nabla\boldsymbol{v}\right\|^2 + \tau\left\|\frac{1}{\sqrt{\rho_{n+1}}}\nabla q\right\|^2\right)^{1/2}. \tag{51}$$

The density equation considered herein is standard, and its unique solvability is well studied (see, *e.g.*, Chap. 5 in the classical monograph [37]). Moreover, since we are not proposing any novel numerics for the density, it will be assumed that ρ_{n+1} is regular enough so that the convective terms in the bilinear form A are well-defined.

Theorem 4.5 (Unique solvability of the nth step of the decoupled scheme)**.** *For $\boldsymbol{f}_{n+1} \in [H^{-1}(\Omega)]^d$, $(\boldsymbol{u}_n, \hat{\mathbf{u}}_n, p_n) \in X \times Y \times Z$, $\mu_{n+1} \in W^{1,\infty}(\Omega)$ and (ρ_{n+1}, ρ_n) sufficiently regular and bounded (20), problem (48) has a unique solution $(\boldsymbol{u}_{n+1}, \hat{\mathbf{u}}_{n+1}, p_{n+1}) \in X \times Y \times Z$ for any $\tau > 0$.*

Proof. We begin by showing that the linear functional f is bounded. For any $(\boldsymbol{v}, \hat{\mathbf{v}}, q) \in X \times Y \times Z$, we can write

$$\begin{aligned} |f(\boldsymbol{v}, \hat{\mathbf{v}}, q)| \leq &\frac{1}{\tau}\left|\left(\sqrt{\rho_n}\hat{\mathbf{u}}_n, \sqrt{\rho_{n+1}}\boldsymbol{v}\right)\right| + \left|\left(\frac{1}{\sqrt{\rho_n}}\nabla p_n, \sqrt{\rho_{n+1}}\,\boldsymbol{v}\right)\right| + \left|\left(\frac{1}{\sqrt{\rho_n}}\nabla p_n, \sqrt{\rho_{n+1}}\,\hat{\mathbf{v}}\right)\right| \\ &+ \tau\left|\left(\frac{1}{\sqrt{\rho_n}}\nabla p_n, \frac{1}{\sqrt{\rho_{n+1}}}\nabla q\right)\right| + \left|\left(\frac{1}{\sqrt{\rho_{n+1}}}\nabla^\top\boldsymbol{u}_n\nabla\mu_{n+1}, \sqrt{\rho_{n+1}}\,\boldsymbol{v}\right)\right| + \left|\langle\boldsymbol{f}_{n+1}, \boldsymbol{v}\rangle\right|. \end{aligned}$$

Using similar inequalities as needed before for the stability analysis, we get

$$\begin{aligned} |f(\boldsymbol{v}, \hat{\mathbf{v}}, q)| \leq &\left(\left\|\sqrt{\frac{\rho_n}{\tau}}\hat{\mathbf{u}}\right\| + \frac{\|\nabla\mu_{n+1}\|_{L^\infty(\Omega)}}{\sqrt{\varrho_{\min}\mu_{\min}/\tau}}\left\|\sqrt{\mu_n}\,\nabla\boldsymbol{u}_n\right\|\right)\left\|\sqrt{\frac{\rho_{n+1}}{\tau}}\boldsymbol{v}\right\| + \frac{\|\boldsymbol{f}_{n+1}\|_{-1}}{\sqrt{\mu_{\min}}}\left\|\sqrt{\mu_{n+1}}\,\nabla\boldsymbol{v}\right\| \\ &+ \left\|\sqrt{\frac{\tau}{\rho_n}}\nabla p_n\right\|\left(\left\|\sqrt{\frac{\rho_{n+1}}{\tau}}\boldsymbol{v}\right\| + \left\|\sqrt{\frac{\rho_{n+1}}{\tau}}\hat{\mathbf{v}}\right\| + \left\|\sqrt{\frac{\tau}{\rho_{n+1}}}\nabla q\right\|\right). \end{aligned}$$

Under the regularity requirements stated in the theorem, all the terms above that do not depend on $(\boldsymbol{v}, \hat{\mathbf{v}}, q)$ are bounded, so there is a positive constant C such that

$$
\begin{aligned}
|f(\boldsymbol{v}, \hat{\mathbf{v}}, q)| &\leq C\left(\frac{1}{\sqrt{\tau}}\left\|\sqrt{\rho_{n+1}}\,\boldsymbol{v}\right\| + \frac{1}{\sqrt{\tau}}\left\|\sqrt{\rho_{n+1}}\,\hat{\mathbf{v}}\right\| + \left\|\sqrt{\frac{\tau}{\rho_{n+1}}}\nabla q\right\| + \sqrt{2}\left\|\sqrt{\mu_{n+1}}\,\nabla\boldsymbol{v}\right\|\right) \\
&\leq 2C\left(\frac{1}{\tau}\left\|\sqrt{\rho_{n+1}}\,\boldsymbol{v}\right\|^2 + \frac{1}{\tau}\left\|\sqrt{\rho_{n+1}}\,\hat{\mathbf{v}}\right\|^2 + \tau\left\|\sqrt{\frac{1}{\rho_{n+1}}}\nabla q\right\|^2 + 2\left\|\sqrt{\mu_{n+1}}\,\nabla\boldsymbol{v}\right\|^2\right)^{1/2} \\
&= 2C|||(\boldsymbol{v}, \hat{\mathbf{v}}, q)|||,
\end{aligned} \tag{52}
$$

where we have used that $a+b+c+d < 2\sqrt{a^2+b^2+c^2+d^2}$ for any $a, b, c, d \in \mathbb{R}$. The continuity of the bilinear A can be showed using similar arguments, so it remains to prove its ellipticity. We have

$$
\begin{aligned}
A((\boldsymbol{v}, \hat{\mathbf{v}}, q), (\boldsymbol{v}, \hat{\mathbf{v}}, q)) = &\frac{1}{\tau}\left\|\sqrt{\rho_{n+1}}\,\boldsymbol{v}\right\|^2 + \left\|\sqrt{\mu_{n+1}}\,\nabla\boldsymbol{v}\right\|^2 + \tau\left\|\frac{1}{\sqrt{\rho_{n+1}}}\nabla q\right\|^2 \\
&+ (\nabla\cdot\boldsymbol{v}, q) + (\nabla q, \hat{\mathbf{v}}) + \frac{1}{\tau}\left(\hat{\mathbf{v}} - \boldsymbol{v}, \rho_{n+1}\hat{\mathbf{v}}\right),
\end{aligned}
$$

where

$$
\begin{aligned}
\left\|\sqrt{\rho_{n+1}}\,\boldsymbol{v}\right\|^2 + \left(\hat{\mathbf{v}} - \boldsymbol{v}, \rho_{n+1}\hat{\mathbf{v}}\right) &= \left\|\sqrt{\rho_{n+1}}\,\boldsymbol{v}\right\|^2 + \left\|\sqrt{\rho_{n+1}}\,\hat{\mathbf{v}}\right\|^2 - \left(\sqrt{\rho_{n+1}}\,\boldsymbol{v}, \sqrt{\rho_{n+1}}\,\hat{\mathbf{v}}\right) \\
&= \frac{1}{2}\left(\left\|\sqrt{\rho_{n+1}}\,\boldsymbol{v}\right\|^2 + \left\|\sqrt{\rho_{n+1}}\,\hat{\mathbf{v}}\right\|^2 + \left\|\sqrt{\rho_{n+1}}(\hat{\mathbf{v}} - \boldsymbol{v})\right\|^2\right)
\end{aligned}
$$

and

$$
\begin{aligned}
(\nabla\cdot\boldsymbol{v}, q) + (\nabla q, \hat{\mathbf{v}}) &= -(\boldsymbol{v}, \nabla q) + (\nabla q, \hat{\mathbf{v}}) \\
&= (\nabla q, \hat{\mathbf{v}} - \boldsymbol{v}) \\
&= \left(\sqrt{\frac{\tau}{\rho_{n+1}}}\nabla q, \sqrt{\frac{\rho_{n+1}}{\tau}}(\hat{\mathbf{v}} - \boldsymbol{v})\right).
\end{aligned}
$$

Hence

$$
\begin{aligned}
A((\boldsymbol{v}, \hat{\mathbf{v}}, q), (\boldsymbol{v}, \hat{\mathbf{v}}, q)) = &\frac{1}{2\tau}\left(\left\|\sqrt{\rho_{n+1}}\,\boldsymbol{v}\right\|^2 + \left\|\sqrt{\rho_{n+1}}\,\hat{\mathbf{v}}\right\|^2\right) + \left\|\sqrt{\mu_{n+1}}\,\nabla\boldsymbol{v}\right\|^2 \\
&+ \tau\left\|\frac{1}{\sqrt{\rho_{n+1}}}\nabla q\right\|^2 + \frac{1}{2\tau}\left\|\sqrt{\rho_{n+1}}(\hat{\mathbf{v}} - \boldsymbol{v})\right\|^2 + \left(\sqrt{\frac{\tau}{\rho_{n+1}}}\nabla q, \sqrt{\frac{\rho_{n+1}}{\tau}}(\hat{\mathbf{v}} - \boldsymbol{v})\right).
\end{aligned}
$$

The last three terms can be combined as

$$
\begin{aligned}
\tau\left\|\frac{1}{\sqrt{\rho_{n+1}}}\nabla q\right\|^2 &+ \frac{1}{2\tau}\left\|\sqrt{\rho_{n+1}}(\hat{\mathbf{v}} - \boldsymbol{v})\right\|^2 + \left(\sqrt{\frac{\tau}{\rho_{n+1}}}\nabla q, \sqrt{\frac{\rho_{n+1}}{\tau}}\,(\hat{\mathbf{v}} - \boldsymbol{v})\right) \\
&= \frac{\tau}{2}\left\|\frac{1}{\sqrt{\rho_{n+1}}}\nabla q\right\|^2 + \frac{1}{2}\left\|\sqrt{\frac{\rho_{n+1}}{\tau}}(\hat{\mathbf{v}} - \boldsymbol{v}) + \sqrt{\frac{\tau}{\rho_{n+1}}}\nabla q\right\|^2.
\end{aligned}
$$

Thus,

$$
\begin{aligned}
A((\boldsymbol{v}, \hat{\mathbf{v}}, q), (\boldsymbol{v}, \hat{\mathbf{v}}, q)) &= \frac{1}{2}|||(\boldsymbol{v}, \hat{\mathbf{v}}, q)|||^2 + \frac{1}{2}\left\|\sqrt{\frac{\rho_{n+1}}{\tau}}(\hat{\mathbf{v}} - \boldsymbol{v}) + \sqrt{\frac{\tau}{\rho_{n+1}}}\nabla q\right\|^2 \\
&\geq \frac{1}{2}|||(\boldsymbol{v}, \hat{\mathbf{v}}, q)|||^2.
\end{aligned} \tag{53}
$$

Therefore, we have the unique solvability of (48) through the Lax–Milgram theorem. □

5. Implementation aspects

5.1. Non-Newtonian models

Variable-density applications often involve generalised Newtonian fluids, where the kinematic viscosity $\nu := \mu/\rho$ may depend on the symmetric velocity gradient. In that case, using ν_{n+1} would introduce a non-linearity in the schemes we have presented. This can be easily overcome by using extrapolation, but some care must be taken. Let us take, for example, the BDF2 scheme. An implicit treatment of the viscosity would mean writing

$$\nu_{n+1} = \nu(\rho_{n+1}, |\nabla^{\mathrm{s}} \boldsymbol{u}_{n+1}|),$$

where the dependence on ρ determines the phase distribution, and the dependence on $|\nabla^{\mathrm{s}} \boldsymbol{u}|$ comes from the rheological model. Although it may be tempting to use the interpolation $\nu_{n+1} \approx \nu_n^\star = 2\nu_n - \nu_{n-1}$, this could produce negative viscosity in some regions. Therefore, we propose instead to consider

$$\nu_{n+1} \approx \nu(\rho_{n+1}, |\nabla^{\mathrm{s}} \boldsymbol{u}_n^\star|) =: \nu_{n+1,n}^\star,$$

that is, extrapolating only the velocity field; of course, we could also extrapolate the density, but there is no need to do that because ρ_{n+1} is already known at the time of tackling the momentum equation.

The second part of the viscous term can also be treated in various ways. Two formally second-order extrapolations are

$$\nabla^\top \boldsymbol{u}_{n+1} \nabla \mu_{n+1} \approx 2\nabla^\top \boldsymbol{u}_n \nabla \mu_n - \nabla^\top \boldsymbol{u}_{n-1} \nabla \mu_{n-1}$$

and

$$\nabla^\top \boldsymbol{u}_{n+1} \nabla \mu_{n+1} \approx \nabla^\top \boldsymbol{u}_n^\star \nabla \left(\rho_{n+1} \nu_{n+1,n}^\star\right).$$

The latter is the approach used in our simulations. Either way, the stability analysis we derived remains unchanged. By contrast, there are certain second-order extrapolations, such as $\nabla^\top \boldsymbol{u}_n^\star \nabla \mu_n^\star$, which may not be as stable because the multiplication of the two extrapolated quantities produces additional, potentially negative terms.

5.2. Finite element implementation

The temporal schemes proposed herein are meant to be general and, in principle, usable in combination with various spatial discretisation frameworks. This section discusses some implementation aspects involving finite element discretisations. We will, however, be concise and not dwell on finite element formalism. For the current discussion, it suffices to state that we consider the unknowns $(\boldsymbol{u}_{n+1}, p_{n+1}, \rho_{n+1})$ and their respective test functions to be in suitable, conforming finite element spaces (X_h, Y_h, Z_h), respectively, defined with respect to a triangulation $\mathcal{T}$ of Ω.

Let us consider the following boundary-condition setting for the Navier–Stokes system:

$$\begin{aligned} \boldsymbol{u} &= \mathbf{v} && \text{in } \Gamma_D \times (0,T], \\ (\mu \nabla \boldsymbol{u})\boldsymbol{n} - p\boldsymbol{n} &= \mathbf{h} && \text{in } \Gamma_N \times (0,T], \end{aligned}$$

where $(\mathbf{v}, \mathbf{h})$ are appropriate data. Taking the first-order coupled scheme as a prototypical setting, the variational formulation for the Navier–Stokes system would be to find $p_{n+1} \in Y_h$ and $\boldsymbol{u}_{n+1} \in X_h$, with $\boldsymbol{u}_{n+1}|_{\Gamma_D} = \mathbf{v}_{n+1}$, such that

$$\begin{aligned} &\left(\frac{\rho_{n+1}}{\tau} \boldsymbol{u}_{n+1} + (\rho_{n+1} \nabla \boldsymbol{u}_{n+1})\, \boldsymbol{u}_n + \frac{1}{2}[\nabla \cdot (\rho_{n+1} \boldsymbol{u}_n)] \boldsymbol{u}_{n+1}, \boldsymbol{w}\right) + (\mu_{n+1} \nabla \boldsymbol{u}_{n+1}, \nabla \boldsymbol{w}) - (p_{n+1}, \nabla \cdot \boldsymbol{w}) \\ &\quad = \frac{1}{\tau}\left(\sqrt{\rho_n \rho_{n+1}}\, \boldsymbol{u}_n, \boldsymbol{w}\right) + \sum_{\Omega_e \in \mathcal{T}} \int_{\Omega_e} (\nabla^\top \boldsymbol{u}_n \nabla \mu_n) \cdot \boldsymbol{w} \, \mathrm{d}\Omega + \int_{\Gamma_N} \mathbf{h}_{n+1} \cdot \boldsymbol{w} \, \mathrm{d}\Gamma + \langle \boldsymbol{f}_{n+1}, \boldsymbol{w} \rangle, \\ &(q, \nabla \cdot \boldsymbol{u}_{n+1}) = 0, \end{aligned}$$

for all $q \in Y_h$ and $\boldsymbol{w} \in X_h$, with $\boldsymbol{w}|_{\Gamma_D} = \boldsymbol{0}$. There are two distinct aspects regarding the explicit part of the viscous term. The first is that, differently from the "Laplacian" part, the explicit one is *not* integrated by parts, which is possible because it does not contain any second-order velocity derivatives. Moreover, we have written the summation over element interiors Ω_e only, since μ may not have enough regularity for the integral over Ω to be formally well-defined. This situation arises, for example, if ν is a function of $\nabla^{\mathrm{s}}\boldsymbol{u}$ and hence discontinuous in the fully discrete case. This formalism, however, has no impact on the implementation, since computing the integrals in each element separately and adding the results is the way finite elements are implemented. Additionally, in the non-Newtonian case the term containing $\nabla\mu$ is only computable if the velocity is approximated with elements of at least second order. If linear elements elements are used, the viscosity gradient needs to be reconstructed in some other way (*e.g.*, through simple projections or local averaging).

An attractive feature of our schemes is that, even in the coupled case, the velocity-velocity matrix is block-diagonal. The fully discrete version of the problem above reads

$$\begin{bmatrix} \mathbf{A}_{n+1} & \mathbf{B}^\top \\ \mathbf{B} & \mathbf{0} \end{bmatrix} \begin{bmatrix} \boldsymbol{U}_{n+1} \\ \boldsymbol{P}_{n+1} \end{bmatrix} = \begin{bmatrix} \boldsymbol{F}_{n+1} \\ \mathbf{0} \end{bmatrix},$$

where $\mathbf{B}$ is the divergence matrix and $\boldsymbol{F}_{n+1}$ is the right-hand side vector depending on ($\boldsymbol{f}_{n+1}$, $\boldsymbol{u}_n, \mu_n, \rho_{n+1}, \rho_n, \mathbf{h}_{n+1}$). The velocity-velocity matrix $\mathbf{A}_{n+1}$ consists of d identical blocks:

$$\mathbf{A}_{n+1} = \begin{bmatrix} \mathbf{K}_{n+1} & \mathbf{0} \\ \mathbf{0} & \mathbf{K}_{n+1} \end{bmatrix} \text{ for } d = 2, \text{ or } \mathbf{A}_{n+1} = \begin{bmatrix} \mathbf{K}_{n+1} & \mathbf{0} & \mathbf{0} \\ \mathbf{0} & \mathbf{K}_{n+1} & \mathbf{0} \\ \mathbf{0} & \mathbf{0} & \mathbf{K}_{n+1} \end{bmatrix} \text{ for } d = 3, \tag{54}$$

where $\mathbf{K}_{n+1} := \mathbf{M}(\rho_{n+1}) + \mathbf{D}(\mu_{n+1}) + \mathbf{C}(\rho_{n+1}, \boldsymbol{u}_n)$, with $\mathbf{M}$, $\mathbf{D}$ and $\mathbf{C}$ denoting, respectively, the mass, diffusion, and convection matrices. The same structure will hold for the BDF2 scheme, with the corresponding extrapolations. The block structure reduces the costs of assembling and solving the linear system – especially in the fractional-step case, where it means that the velocity components can be solved separately.

6. Numerical examples

In this section, we assess the accuracy and stability of our methods through various numerical experiments. All the examples use quadrilateral Lagrangian finite elements with first order for pressure and for density, and second order for velocity. We write the body force as $\boldsymbol{f} = \rho\boldsymbol{g}$, where $\boldsymbol{g}$ is a given gravity field.

Since the second and third tests feature very steep density gradients, we use least-squares methods for the density equation [7]. Mind, however, that while least-squares formulations yield unconditional temporal stability when combined with BDF1 or Crank–Nicolson [38], there is currently no theory available on BDF2.

6.1. Convergence test

To verify the order of convergence of our schemes, we have derived an analytical solution. Considering $\boldsymbol{f} = \mathbf{0}$ and the viscosity field

$$\mu(x, y, t) = Af'(t)\mathrm{e}^{\kappa f(t)} \left[\mathrm{Ei}\left(-\frac{x^2 + y^2}{2/\kappa}\right) + B\right],$$

with Ei denoting the exponential integral function, it is possible to verify that

$$\begin{aligned} \rho(x, y, t) &= 4A \exp\left[\kappa\left(f(t) - \frac{x^2 + y^2}{2}\right)\right], \\ p(x, y, t) &= -2Af''(t)\mathrm{e}^{\kappa f(t)} \left[\mathrm{Ei}\left(-\frac{x^2 + y^2}{2/\kappa}\right) + C\right], \\ \boldsymbol{u}(x, y, t) &= \frac{f'(t)}{x^2 + y^2} \begin{pmatrix} x \\ y \end{pmatrix} \end{aligned}$$

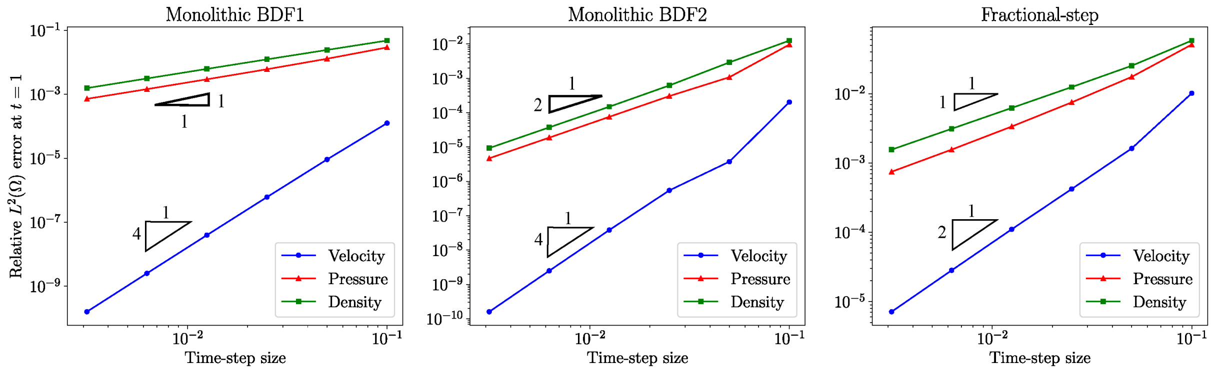

FIGURE 1. Convergence study for monolithic BDF1 (*left*), monolithic BDF2 (*centre*), and fractional-step (*right*) schemes, confirming (at least) first-order convergence in the BDF1 and fractional-step schemes, and second-order convergence in the BDF2 scheme for all unknowns.

solves the incompressible variable-density Navier–Stokes system for any combination of $A > 0$, $B, C, \kappa \in \mathbb{R}$ and $f(t) : \mathbb{R} \to \mathbb{R}$ such that $\mu > 0$ in $\bar{Q}$. For the test case, we set $A = 1$, $B = 1$, $\kappa = -2$ and $f(t) = 2t - \sin t$, and the domain is a quarter annulus with inner and outer radii $r = 0.5$ and $R = 1$, respectively, centred at the origin. With that, the pressure scaling $\int_\Omega p \, \mathrm{d}\Omega = 0$ corresponds to

$$C = \frac{R^2 \mathrm{Ei}(R^2) - r^2 \mathrm{Ei}(r^2) + \mathrm{e}^{r^2} - \mathrm{e}^{R^2}}{r^2 - R^2} \approx -0.79533.$$

The initial and boundary conditions are computed from the analytical solution; since this is a purely radial flow moving away from the centre, density boundary conditions are only prescribed along the inner radial wall. For a final time $T = 1$, starting with a mesh with 6×10 elements (in the radial and angular directions, respectively) and $\tau = 0.1$, we perform a uniform refinement study halving both τ and the mesh size h at each level. As shown in Figure 1, the convergence rates of all unknowns are at least quadratic for BDF2 and at least linear for the first-order schemes, as expected; the velocity shows some superconvergence, which is often observed for problems with smooth solutions [22,39].

6.2. Rayleigh–Taylor instability

The next test is a popular benchmark for variable-density flow solvers, namely the Rayleigh–Taylor instability [1]. The setup has two fluids initially at rest in $\Omega = (0, a/2) \times (-2a, 2a)$, under gravity $\boldsymbol{g} = (0, -g)^\top$. Fluid 2 sits initially on top of fluid 1 and is denser ($\rho_2 = 3\rho_1$). While the standard setup found in the literature uses constant μ, we assume instead constant ν so that $\mu = \nu\rho$ can vary. The goal is to test the IMEX treatment of variable μ and $\nabla^\top \boldsymbol{u}$, which is the key novelty of our methods. The initial density field is

$$\rho|_{t=0} = \frac{\rho_2 + \rho_1}{2} + \frac{\rho_2 - \rho_1}{2} \tanh\left(100\frac{y}{a} + 10\cos\frac{2\pi x}{a}\right).$$

We make the results dimensionless through the following reference quantities: ν for viscosity, ρ_1 for density, a for length, and $\sqrt{ag}$ for velocity, which yields $\sqrt{a/g}$ as temporal scale. The flow regime is fully parametrised by the Reynolds and Atwood numbers

$$\mathrm{Re} = \frac{a\sqrt{ag}}{\nu} = 1000 \quad \text{and} \quad \mathrm{At} = \left|\frac{\rho_2 - \rho_1}{\rho_2 + \rho_1}\right| = \frac{1}{2}.$$

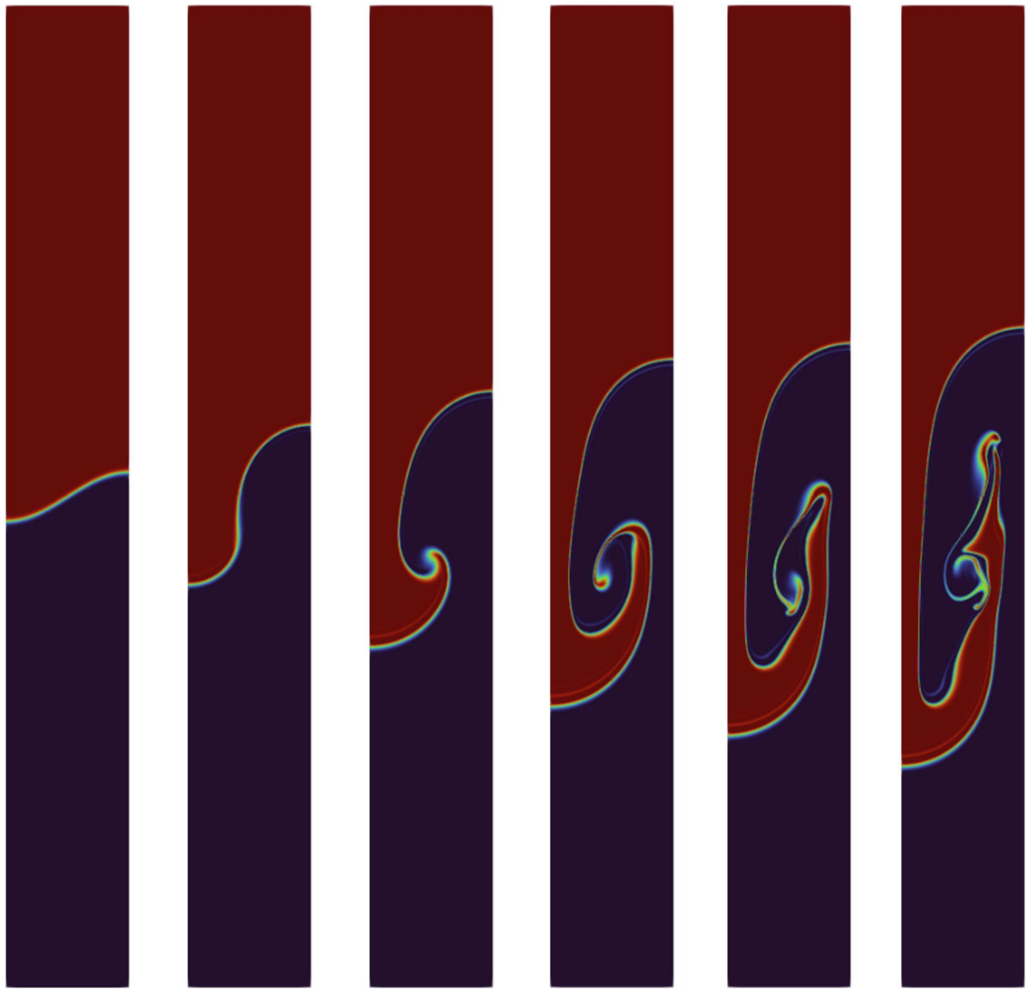

FIGURE 2. Rayleigh–Taylor instability: snapshots of the density field for $t = 0, 1.4, 2.1, 2.45, 2.8$ and 3.15.

The top and bottom walls are no-slip boundaries, while symmetry (free slip) is enforced on the sides. For the simulation, we use a mesh consisting of 100×800 elements. The time-step size, $\tau = 0.001$, is at least an order of magnitude larger than what is often seen in the literature [1, 16], which is possible because our schemes are unconditionally stable. The density field obtained with the second-order scheme presented in Section 3.2 is shown in Figure 2 for different times. Since our objective was to test the temporal stability of the scheme, we have not used any extra stabilisation. This explains why small oscillations appear around the interface, but despite this, the results show a stable behaviour even with the large time-step size.

Finally, in Figure 3 we show the temporal evolution of the height H of the rising bubble. For comparison, we have reported our results alongside those of Guermond and Quartapelle [1] (although in their work the viscosity μ was taken as constant), and those by Tryggvason [40]. We can observe that the three sets of results are in good agreement.

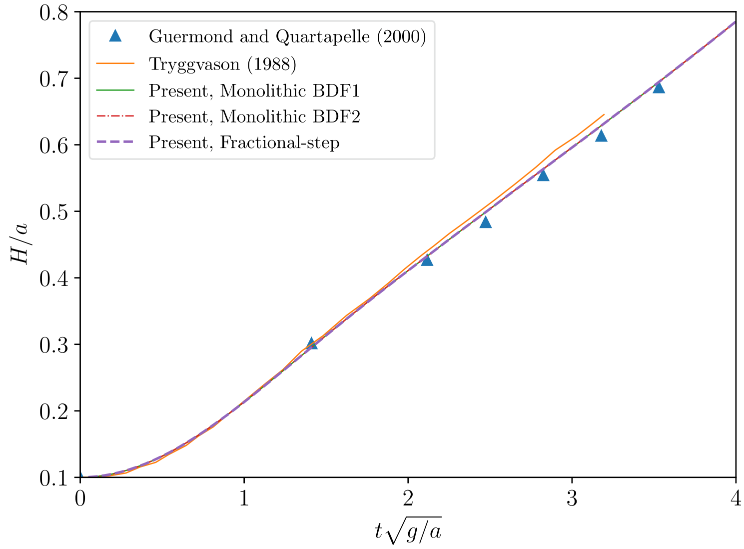

FIGURE 3. Rayleigh–Taylor instability: height of the rising bubble on the right wall.

6.3. Viscoplastic falling droplet

The last example is inspired by the classical falling droplet benchmark [41], but we here consider one of the fluids as viscoplastic using the regularised Bingham model [42]

$$\nu(\dot{\gamma}) = \nu_\infty + \frac{\sigma_0}{\rho_\infty} \frac{1 - \mathrm{e}^{-m\dot{\gamma}}}{\dot{\gamma}}, \quad \dot{\gamma} := \sqrt{2\nabla^{\mathrm{s}}\boldsymbol{u} : \nabla^{\mathrm{s}}\boldsymbol{u}}.$$

For the non-regularised version ($m \to \infty$), the material behaves as a Newtonian fluid with viscosity ν_∞ wherever the viscous stress surpasses the yield stress σ_0, but behaves like a solid ($\nu \to \infty$) otherwise. Our setup considers a heavy viscoplastic droplet ($\rho_\infty = 100$) immersed in a lighter fluid ($\rho_f = 1$), which sits on a layer of the viscoplastic fluid (further details on the geometric setup can be found in reference works [41]). The system is initially at rest and then moves under gravitational force $\boldsymbol{f} = (0, -\rho)^\top$. Free slip is imposed on the entire boundary, which on the lateral walls serves to enforce symmetry. We set $\nu_\infty = 10^{-3}$, $\sigma_0 = 1$ and $m = 50$. The time-step size is $\tau = 0.005$, and the mesh contains 200×800 square elements.

This is a challenging problem to simulate, due to the large density ratio between the fluids and to the sharp viscosity gradients caused by viscoplasticity. All three IMEX schemes produced similar results, so in Figure 4 we show only the solution of the fractional-step method. The snapshots of the viscosity field reveal that the droplet is essentially solid until shortly before impact with the lower layer. During impact, the lower layer fluidises, but then starts hardening again from the bottom. Again, this last example highlights that no numerical instabilities were found and demonstrates that the proposed methodology can cope with complex physical situations.

7. Concluding remarks

In this article, we have devised, analysed, and assessed different IMEX schemes for the incompressible variable-density Navier–Stokes system. While previous references assume constant viscosity for the analysis, we have considered the more realistic case of variable viscosity, focusing on the IMEX treatment of the diffusive term. Our approach is fully linearised and makes the velocity subsystem block-diagonal. This is especially attractive in the fractional-step case because, at each time step, the resulting system is split into simple, scalar subproblems.

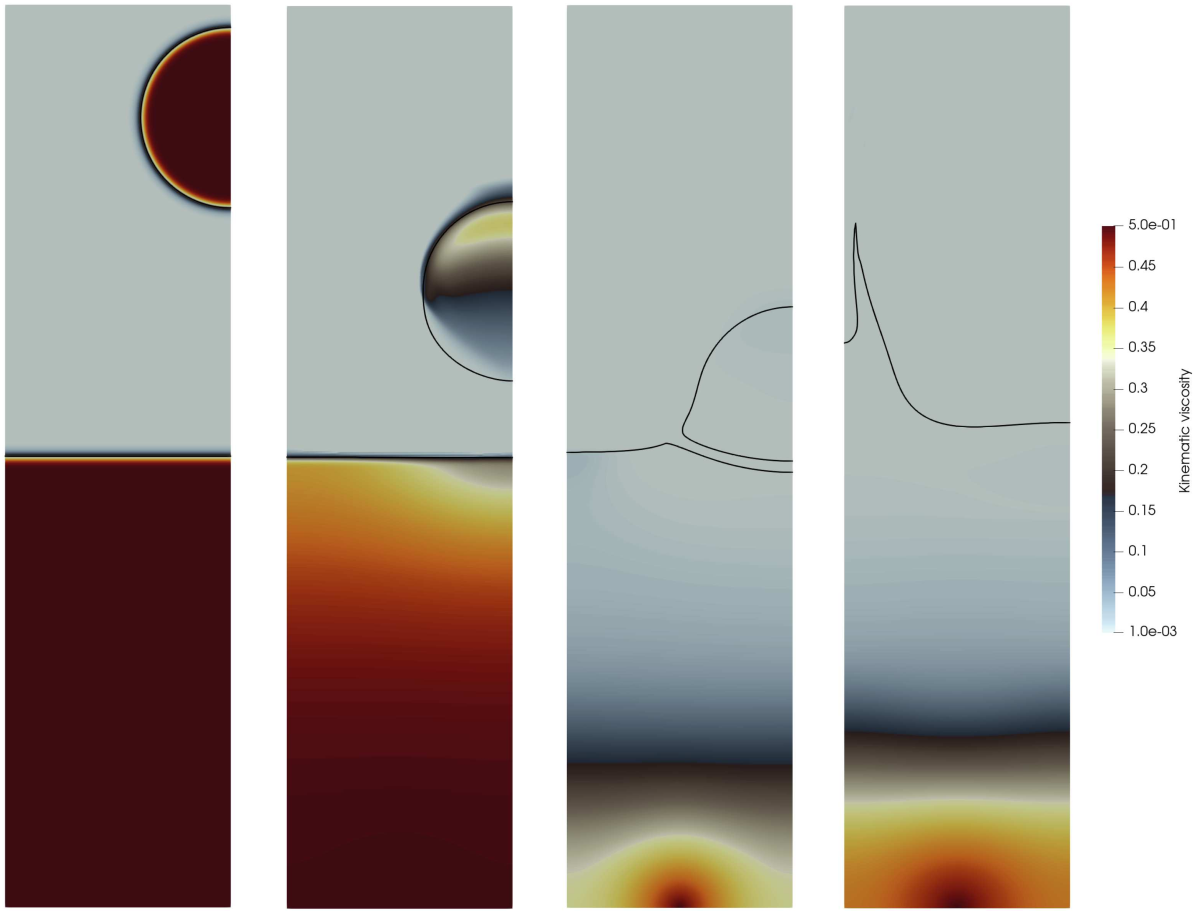

FIGURE 4. Viscoplastic falling droplet: snapshots of the viscosity field ν, for $t = 0, 0.9, 1.15$ and 1.5. The black contour lines show the interface ($\rho = \frac{100+1}{2}$).

These features can simplify implementation and increase efficiency. The unconditional temporal stability of our schemes is shown not only through rigorous discrete-in-time analysis but also *via* challenging numerical examples. There are, nevertheless, problems that remain open. Throughout the analysis, we have assumed that the density is positive and bounded everywhere at all times, a condition which – although standard in the literature – is not trivial. Therefore, we plan to address this matter soon by employing state-of-the-art bound-preserving numerical techniques [29, 30] to evolve the density. We will also work on discretisations to enforce the Lipschitz condition for the dynamic viscosity μ, which in general depends on the density ($\mu = \rho\nu$). The design and analysis of such schemes in the fully discrete setting is an interesting open problem, especially for flows with large density jumps.

ACKNOWLEDGMENTS

NEC and DRQP acknowledge funding by the Federal Ministry of Education and Research (BMBF) and the Ministry of Culture and Science of the German State of North Rhine-Westphalia (MKW) under the Excellence Strategy of the Federal Government and the Länder.

Funding

The work of GRB has been partially funded by the Leverhulme Trust through the Research Project Grant No. RPG-2021-238. EC acknowledges the support given by the Agencia Nacional de Investigación y Desarrollo (ANID) through the project FONDECYT 1210156 and the support given by DICYT-USACH.

Data availability statement

The research data associated with this article are included in the article.

References

[1] J.-L. Guermond and L. Quartapelle, A projection FEM for variable density incompressible flows. *J. Comput. Phys.* **165** (2000) 167–188.

[2] J.-L. Guermond and A.J. Salgado, Error analysis of a fractional time-stepping technique for incompressible flows with variable density. *SIAM J. Numer. Anal.* **49** (2011) 917–944.

[3] R. An, Error analysis of a new fractional-step method for the incompressible Navier–Stokes equations with variable density. *J. Sci. Comput.* **84** (2020) 3.

[4] H. Chen, J. Mao and J. Shen, Error estimate of Gauge–Uzawa methods for incompressible flows with variable density. *J. Comput. Appl. Math.* **364** (2020) 112321.

[5] W. Cai, B. Li and Y. Li, Error analysis of a fully discrete finite element method for variable density incompressible flows in two dimensions. *ESAIM: Math. Modell. Numer. Anal.* **55** (2021) S103–S147.

[6] J. Deteix, G.L. Ndetchoua Kouamo and D. Yakoubi, A new energy stable fractional time stepping scheme for the Navier–Stokes/Allen–Cahn diffuse interface model. *Comput. Methods Appl. Mech. Eng.* **393** (2022) 114759.

[7] J.-H. Pyo and J. Shen, Gauge–Uzawa methods for incompressible flows with variable density. *J. Comput. Phys.* **221** (2007) 181–197.

[8] C. Liu, J. Shen and X. Yang, Decoupled energy stable schemes for a phase-field model of two-phase incompressible flows with variable density. *J. Sci. Comput.* **62** (2015) 601–622.

[9] J.-L. Guermond and A.J. Salgado, A splitting method for incompressible flows with variable density based on a pressure Poisson equation. *J. Comput. Phys.* **228** (2009) 2834–2846.

[10] A.J. Salgado, A diffuse interface fractional time-stepping technique for incompressible two-phase flows with moving contact lines. *ESAIM: Math. Modell. Numer. Anal.* **47** (2013) 743–769.

[11] O. Axelsson, X. He and M. Neytcheva, Numerical solution of the time-dependent Navier–Stokes equation for variable density-variable viscosity. Part I. *Math. Model. Anal.* **20** (2015) 232–260.

[12] L. Cappanera, J.-L. Guermond, W. Herreman and C. Nore, Momentum-based approximation of incompressible multiphase fluid flows. *Int. J. Numer. Methods Fluids* **86** (2018) 541–563.

[13] V. A and L. Cappanera, Stability and error analysis of a semi-implicit scheme for incompressible flows with variable density and viscosity. *J. Numer. Math.* **33** (2025) 161–186.

[14] J. Wu, J. Shen and X. Feng, Unconditionally stable Gauge–Uzawa finite element schemes for incompressible natural convection problems with variable density. *J. Comput. Phys.* **348** (2017) 776–789.

[15] M. Li, Y. Cheng, J. Shen and X. Zhang, A bound-preserving high order scheme for variable density incompressible Navier–Stokes equations. *J. Comput. Phys.* **425** (2021) 109906.

[16] D.R.Q. Pacheco and R. Schussnig, Consistent pressure Poisson splitting methods for incompressible multi-phase flows: eliminating numerical boundary layers and inf-sup compatibility restrictions. *Comput. Mech.* **70** (2022) 977–992.

[17] S. Gottlieb and C. Wang, Stability and convergence analysis of fully discrete Fourier collocation spectral method for 3-D viscous Burgers' equation. *J. Sci. Comput.* **53** (2012) 102–128.

[18] K. Cheng and C. Wang, Long time stability of high order multistep numerical schemes for two-dimensional incompressible Navier–Stokes equations. *SIAM J. Numer. Anal.* **54** (2016) 3123–3144.

[19] E. Burman and J. Guzmán, Implicit-explicit multistep formulations for finite element discretisations using continuous interior penalty. *ESAIM: Math. Modell. Numer. Anal.* **56** (2022) 349–383.

[20] E. Burman, D. Garg and J. Guzmán, Implicit-explicit time discretization for Oseen's equation at high Reynolds number with application to fractional step methods. *SIAM J. Numer. Anal.* **61** (2023) 2859–2886.

[21] E. Burman, D. Garg and J. Guzmán, Implicit-explicit Crank–Nicolson scheme for Oseen's equation at high Reynolds number. *Math. Models Methods Appl. Sci.* In press (2024).

[22] G.R. Barrenechea, E. Castillo and D.R.Q. Pacheco, Implicit-explicit schemes for incompressible flow problems with variable viscosity. *SIAM J. Sci. Comput.* **46** (2024) A2660–A2682.

[23] J. Stiller, A spectral deferred correction method for incompressible flow with variable viscosity. *J. Comput. Phys.* **423** (2020) 109840.

[24] M. Guesmi, M. Grotteschi and J. Stiller, Assessment of high-order IMEX methods for incompressible flow. *Int. J. Numer. Methods Fluids* **95** (2023) 954–978.

[25] M. El-Amrani, A. Obbadi, M. Seaid and D. Yakoubi, Error estimates for a viscosity-splitting scheme in time applied to non-Newtonian fluid flows. *Comput. Methods Appl. Mech. Eng.* **419** (2024) 116639.

[26] A. Ern and J.-L. Guermond, Finite Elements I. Springer (2021).

[27] J.G. Heywood and R. Rannacher, Finite-element approximation of the nonstationary Navier–Stokes problem. Part IV: error analysis for second-order time discretization. *SIAM J. Numer. Anal.* **27** (1990) 353–384.

[28] E. Burman, A monotonicity preserving, nonlinear, finite element upwind method for the transport equation. *Appl. Math. Lett.* **49** (2015) 141–146.

[29] D. Kuzmin and H. Hajduk, Property-preserving Numerical Schemes for Conservation Laws. World Scientific, Singapore (2023).

[30] G.R. Barrenechea, V. John and P. Knobloch, Monotone Discretizations for Elliptic Second Order Partial Differential Equations. Vol. 61. Springer Nature (2025).

[31] E. Burman and A. Ern, A nonlinear consistent penalty method weakly enforcing positivity in the finite element approximation of the transport equation. *Comput. Methods Appl. Mech. Eng.* **320** (2017) 122–132.

[32] A. Amiri, G.R. Barrenechea and T. Pryer, A nodally bound-preserving finite element method for reaction–convection–diffusion equations. *Math. Models Methods Appl. Sci.* **34** (2024) 1533–1565.

[33] J.L. Guermond, P. Minev and J. Shen, An overview of projection methods for incompressible flows. *Comput. Methods Appl. Mech. Eng.* **195** (2006) 6011–6045.

[34] V. John and J. Novo, Analysis of the pressure stabilized Petrov–Galerkin method for the evolutionary Stokes equations avoiding time step restrictions. *SIAM J. Numer. Anal.* **53** (2015) 1005–1031.

[35] C. Wang, J. Wang, Z. Xia and L. Xu, Optimal error estimates of a Crank–Nicolson finite element projection method for magnetohydrodynamic equations. *ESAIM: Math. Modell. Numer. Anal.* **56** (2022) 767–789.

[36] C. Wang, J. Wang, S.M. Wise, Z. Xia and L. Xu, Convergence analysis of a temporally second-order accurate finite element scheme for the Cahn–Hilliard–Magnetohydrodynamics system of equations. *J. Comput. Appl. Math.* **436** (2024) 115409.

[37] A. Ern and J.-L. Guermond, Theory and Practice of Finite Elements. Vol. 159. Springer New York (2004).

[38] D.R.Q. Pacheco and O. Steinbach, On the initial higher-order pressure convergence in equal-order finite element discretizations of the Stokes system. *Comput. Math. Appl.* **109** (2022) 140–145.

[39] H. Eichel, L. Tobiska and H. Xie, Supercloseness and superconvergence of stabilized low-order finite element discretizations of the Stokes Problem. *Math. Comput.* **80** (2011) 697–697.

[40] G. Tryggvason, Numerical simulations of the Rayleigh–Taylor instability. *J. Comput. Phys.* **75** (1988) 253–282.

[41] C. Calgaro, E. Creusé, T. Goudon and S. Krell, Simulations of non homogeneous viscous flows with incompressibility constraints. *Math. Comput. Simul.* **137** (2017) 201–225.

[42] T.C. Papanastasiou, Flows of materials with yield. *J. Rheol.* **31** (1987) 385–404.

Please help to maintain this journal in open access!

This journal is currently published in open access under the Subscribe to Open model (S2O). We are thankful to our subscribers and supporters for making it possible to publish this journal in open access in the current year, free of charge for authors and readers.

Check with your library that it subscribes to the journal, or consider making a personal donation to the S2O programme by contacting subscribers@edpsciences.org.

More information, including a list of supporters and financial transparency reports, is available at https://edpsciences.org/en/subscribe-to-open-s2o.